The ANL-Osaka Partial-Wave Amplitudes of πN and γN Reactions

H. Kamano[1], T.-S. H. Lee[2], S.X. Nakamura[3], T. Sato[1]
[1] Research Center for Nuclear Physics, 10-1 Mihogaoka, Ibaraki, Osaka, Japan
[2]Physics Division, Argonne National Laboratory, Argonne, Illinois 60249, USA
[3] University of Science and Technology of China, Hefei, 230026, People's Republic of China

Contact Person: T.-S. H. Lee (email:tshlee@anl.gov), September 20, 2019
(**https://www.phy.anl.gov/theory/research/anl-osaka-pwa**)

Abstract

The determination of the Argonne National Laboratory-Osaka University (ANL-Osaka) Partial-Wave Amplitudes (PWA) of πN and γN Reactions is reviewed. The predicted PWA are presented on a web page (**https://www.phy.anl.gov/theory/research/anl-osaka-pwa**). The formula are given for using the predicted PWA to calculate the cross sections of (1)meson-baryon (MB) scattering $MB \to M'B'$ with $MB, M'B' = \pi N, \eta N, K\Lambda, K\Sigma$, (2) two-pion production $\pi N \to \pi\Delta, \rho N, \sigma N \to \pi\pi N$, (3) Meson photoproduction $\gamma N \to \pi N, \eta N, K\Lambda, K\Sigma$, (4) Pion electroproduction $N(e, e'\pi)N$, (5) inclusive $N(e, e')X$. We also present sample results from our fits to the data.

I. INTRODUCTION

The Argonne National Laboratory-Osaka University (ANL-Osaka) collaboration started in 1996 with a publication [1] of a meson-exchange model for investigating the excitation of the Δ (1232) resonance in πN and γN reactions. The predictions [1, 2] from this model, called the Sato-Lee (SL) model in the community, were found to be consistent with the data from MIT-Bates, Mainz, Bonn, and JLab. The results from the SL model strongly suggested that a dynamical model based on a Hamiltonian with bare N^* states and meson-exchange mechanisms can be used to

1. describe the data of πN and γN reactions up to invariant mass $W = 2$ GeV,

2. extract the masses and widths of nucleon resonances (N^*) from the predicted Partial-Wave Amplitudes (PWA) for investigating the structure of the nucleon and its excited states,

3. apply the constructed Hamiltonian with meson and N^* degrees of freedom to predict the cross sections of the production of mesons $(\pi, 2\pi, \eta, K)$ from nuclei, which are needed for analyzing the data of nuclear reactions induced by hadrons, electrons, and neutrinos in the nucleon resonance region.

The formulation of the SL model was then extended to include the higher mass bare N^* states and the meson-baryon channels which have significant contributions to the πN

and γN total cross sections below invariant mass $W = 2$ GeV. Exploratory calculations using this Dynamical Coupled-Channel (DCC) model were carried out by the ANL-Osaka collaboration during 2004-2006. The analysis of the world data of πN and γN reactions up to $W = 2$ GeV was then carried out at the Excited Baryon Analysis Center (EBAC) at JLab during 2006-2012, with 12 publications [3-15]. The ANL-Osaka collaboration continued the analysis to extract [16, 17] 22 nucleon resonances during 2013-2016. The calculations for the analysis involved solving coupled-channel scattering equations with 8 channels: $\gamma N, \pi N, \eta N, K\Lambda, K\Sigma$, and $\pi\pi N$ which has $\pi\Delta, \sigma N, \rho N$ resonant components. The parameters of the model were determined by performing χ^2-fits to the world data of $\gamma N, \pi N \to \pi N, \eta N, K\Lambda, K\Sigma$ (about 30,000 data points). The ANL-Osaka model was also extended[18] to investigate the neutrino-induced meson production reactions on the nucleon. The computation resources from DOE's NERSC (about 500,000 hours/year) and Argonne's LCRC (about 300,000 hours/year) had been used to complete this task.

The results presented on **https://www.phy.anl.gov/theory/research/anl-osaka-pwa** are for the nuclear and hadron physics communities to get access to the predicted partial-wave amplitudes of $\gamma N, \pi N \to \pi N, \eta N, K\Lambda, K\Sigma, \pi\Delta, \sigma N, \rho N$. In section II, we describe briefly the ANL-Osaka DCC model and the resulting formulation of πN and γN reactions. The procedures for extracting nucleon resonances are given in section III. In section IV, we present formula for using the PWA posted on the web page to calculate the cross sections of the considered meson-baryon reactions . The data included in the fits are summarized in section V. In section VI and Appendix, we present sample results from our fits to the data.

II. ANL-OSAKA DCC MODEL

The ANL-Osaka DCC Model is based on an effective Hamiltonian of the following $energy - independent$ form:

$$H = H_0 + v_{22} + \Gamma_V + h_{\pi\pi N}\,, \tag{1}$$

where $H_0 = \sum_\alpha \sqrt{m_\alpha^2 + \vec{p}_\alpha^{\,2}}$ with m_α and $\vec{p}_\alpha$ denoting the mass and momentum of particle α, respectively. The interactions are defined as

$$v_{22} = \sum_{MB,M'B'} v_{MB,M'B'} + v_{\pi\pi,\pi\pi}\ , \tag{2}$$

$$\Gamma_V = \{\sum_{N^*}(\sum_{MB}\Gamma_{N^*\to MB}) + \sum_{M^*} h_{M^*\to\pi\pi}\} + \{c.c\}\ , \tag{3}$$

$$h_{\pi\pi N} = \{v_{\pi N,\pi\pi N} + v_{\gamma N,\pi\pi N}\} + \{c.c\}\ , \tag{4}$$

where $v_{MB,M'B'}$ is the meson-baryon (MB) interactions, $v_{\pi\pi,\pi\pi}$ is the $\pi\pi$ interactions, $\Gamma_{N^*\to MB}$ describes the decay of a $bare$ excited nucleon (N^*) into a MB state, $h_{M^*\to\pi\pi}$ describes the decay of a $bare$ meson (M^*) into a $\pi\pi$ state, and $\{c.c.\}$ denotes the complex conjugate of the terms on its left-side. For describing the πN and γN reactions up to invariant mass $W = 2$ GeV, we include $MB = \gamma N, \pi N, \eta N, K\Lambda, K\Sigma, \pi\Delta, \rho N, \sigma N$, about 20 bare N^* states, and $M^* = \rho, \sigma$.

A. Hadronic amplitudes

Starting with the Hamiltonian defined by Eqs. (1)-(4), we apply [4] the projection operator method to cast the partial-wave amplitudes of the scattering T matrix of the meson-baryon reaction, $M(\vec{k}) + B(-\vec{k}) \to M'(\vec{k}') + B'(-\vec{k}')$, into the following form

$$T_{M'B',MB}(k',k;E) = t_{M'B',MB}(k',k;E) + t^R_{M'B',MB}(k',k;E), \tag{5}$$

where E is the total energy, k and k' are the meson-baryon relative momenta in the center of mass frame, and $MB, M'B' = \pi N, \eta N, \pi\Delta, \rho N, \sigma N, K\Lambda, K\Sigma$ are the reaction channels included in the analysis. The notation MB also represents the partial-wave quantum numbers: $[L(s_M s_B)S]JT]$, where J is the total angular momentum, T the total isospin, L the orbital angular momentum, S the total spin which is from the coupling of the meson spin s_M and the baryon spin s_B.

The direct reaction amplitude $t_{M'B',MB}(k',k;E)$ in Eq. (5) is defined by a set of coupled-channel equations

$$\begin{aligned} t_{M'B',MB}(k',k;E) \;=\; & V_{M'B',MB}(k',k;E) \\ & + \sum_{M''B''} \int_{C_{M''B''}} k''^2 dk'' V_{M'B',M''B''}(k',k'';E) \\ & \times G_{M''B''}(k'';E) t_{M''B'',MB}(k'',k;E). \end{aligned} \tag{6}$$

Here $C_{M''B''}$ is the integration path, which is taken from 0 to ∞ for the physical E; the summation $\sum_{MB}$ runs over the orbital angular momentum and total spin indices for all MB channels allowed in a given partial wave; $G_{M''B''}(k;E)$ are the meson-baryon Green functions. Defining $E_\alpha(k) = [m_\alpha^2 + k^2]^{1/2}$ with m_α being the mass of a particle α, the meson-baryon Green functions in the above equations are:

$$G_{MB}(k;E) = \frac{1}{E - E_M(k) - E_B(k) + i\epsilon}\,, \tag{7}$$

for the stable πN, ηN, $K\Lambda$, and $K\Sigma$ channels, and

$$G_{MB}(k;E) = \frac{1}{E - E_M(k) - E_B(k) - \Sigma_{MB}(k;E)}\,, \tag{8}$$

for the unstable $\pi\Delta$, ρN, and σN channels. The self energy $\Sigma_{MB}(k;E)$ in Eq. (8) is calculated from a vertex function defining the decay of the considered unstable particle in the presence of a spectator π or N with momentum k. For the $\pi\Delta$ and ρN channels, the self-energies are explicitly given by

$$\Sigma_{\pi\Delta}(k;E) \;=\; \frac{m_\Delta}{E_\Delta(k)} \int q^2 dq \frac{M_{\pi N}(q)}{[M^2_{\pi N}(q) + k^2]^{1/2}} \frac{|f_{\Delta\to\pi N}(q)|^2}{E - E_\pi(k) - [M^2_{\pi N}(q) + k^2]^{1/2} + i\epsilon}, \tag{9}$$

$$\Sigma_{\rho N}(k;E) \;=\; \frac{m_\rho}{E_\rho(k)} \int q^2 dq \frac{M_{\pi\pi}(q)}{[M^2_{\pi\pi}(q) + k^2]^{1/2}} \frac{|f_{\rho\to\pi\pi}(q)|^2}{E - E_N(k) - [M^2_{\pi\pi}(q) + k^2]^{1/2} + i\epsilon}, \tag{10}$$

where $m_\Delta = 1280$ MeV, $m_\rho = 812$ MeV, $M_{\pi N}(q) = E_\pi(q) + E_N(q)$, and $M_{\pi\pi}(q) = E_\pi(q) + E_\pi(q)$. The form factors $f_{\Delta\to\pi N}(q)$ and $f_{\rho\to\pi\pi}(q)$ are for describing the $\Delta \to \pi N$ and $\rho \to \pi\pi$

decays in the Δ and ρ rest frames, respectively. They are parametrized as:

$$f_{\Delta\to\pi N}(q) = -i\frac{(0.98)}{[2(m_N+m_\pi)]^{1/2}}\left(\frac{q}{m_\pi}\right)\left(\frac{1}{1+[q/(358\text{ MeV})]^2}\right)^2, \tag{11}$$

$$f_{\rho\to\pi\pi}(q) = \frac{(0.6684)}{\sqrt{m_\pi}}\left(\frac{q}{(461\text{ MeV})}\right)\left(\frac{1}{1+[q/(461\text{ MeV})]^2}\right)^2. \tag{12}$$

The σ self-energy $\Sigma_{\sigma N}(k;E)$ is calculated from a $\pi\pi$ s-wave scattering model with a vertex function $g(q)$ for the $\sigma\to\pi\pi$ decay and a separable interaction $v(q',q)=h_0h(q')h(q)$. The resulting form is

$$\Sigma_{\sigma N}(k;E) = \langle gG_{\pi\pi}g\rangle(k;E)+\tau(k;E)[\langle gG_{\pi\pi}h\rangle(k;E)]^2, \tag{13}$$

with

$$\tau(k;E) = \frac{h_0}{1-h_0\langle hG_{\pi\pi}h\rangle(k;E)}, \tag{14}$$

$$\langle hG_{\pi\pi}h\rangle(k;E) = \int dqq^2\frac{M_{\pi\pi}(q)}{[M_{\pi\pi}^2(q)+k^2]^{1/2}} \times\frac{h(q)^2}{E-E_N(k)-[M_{\pi\pi}^2(q)+k^2]^{1/2}+i\varepsilon}, \tag{15}$$

$$\langle gG_{\pi\pi}g\rangle(k;E) = \frac{m_\sigma}{E_\sigma(k)}\int dqq^2\frac{M_{\pi\pi}(q)}{[M_{\pi\pi}^2(q)+k^2]^{1/2}} \times\frac{g(q)^2}{E-E_N(k)-[M_{\pi\pi}^2(q)+k^2]^{1/2}+i\varepsilon}, \tag{16}$$

$$\langle gG_{\pi\pi}h\rangle(k;E) = \sqrt{\frac{m_\sigma}{E_\sigma(k)}}\int dqq^2\frac{M_{\pi\pi}(q)}{[M_{\pi\pi}^2(q)+k^2]^{1/2}} \times\frac{g(q)h(q)}{E-E_N(k)-[M_{\pi\pi}^2(q)+k^2]^{1/2}+i\varepsilon}. \tag{17}$$

In the above equations, $m_\sigma=700.0$ MeV and the form factors are

$$g(p) = \frac{g_0}{\sqrt{m_\pi}}\frac{1}{1+(cp)^2}, \tag{18}$$

$$h(p) = \frac{1}{m_\pi}\frac{1}{1+(dp)^2}. \tag{19}$$

where $g_0=1.638$, $h_0=0.556$, $c=1.02$ fm, and $d=0.514$ fm.

The driving terms of Eq. (6) are

$$V_{M'B',MB}(k',k;E) = v_{M'B',MB}(k',k)+Z^{(E)}_{M'B',MB}(k',k;E)\,, \tag{20}$$

where $v_{M'B',MB}(k',k)$ are the meson-exchange potentials derived from the tree-diagrams, as illustrated in Fig. 1, of phenomenological Lagrangians. Within the unitary transformation method used in the derivation, those potentials are energy independent and free of singularities. The Lagrangians used in our derivations and the partial-wave expansions of $v_{M'B',MB}(k',k)$ are given in Appendices B and C of Ref. [16].

The energy-dependent $Z^{(E)}_{M'B',MB}(k',k;E)$ terms in Eq. (20), as illustrated in Fig. 2, contain the *moving* singularities due to the $\pi\pi N$ cuts. The procedures for evaluating the partial-wave matrix elements of $Z^{(E)}_{M'B',MB}(k',k;E)$ are explained in detail in the Appendix E of Ref. [4].

The second term in the right-hand-side of Eq. (5) is the N^*-excitation amplitude defined by

$$t^R_{M'B',MB}(k',k;E) = \sum_{N^*_n,N^*_m} \bar{\Gamma}_{M'B',N^*_n}(k';E)[D(E)]_{n,m}\bar{\Gamma}_{N^*_m,MB}(k;E). \tag{21}$$

Here the dressed $N^* \to MB$ and $MB \to N^*$ decay vertices are, respectively, defined by

$$\bar{\Gamma}_{MB,N^*}(k;E) = \Gamma_{MB,N^*}(k) + \sum_{M'B'} \int q^2 dq t_{MB,M'B'}(k,q;E) G_{M'B'}(q,E)\Gamma_{M'B',N^*}(q), \tag{22}$$

$$\bar{\Gamma}_{N^*,MB}(k;E) = \Gamma^\dagger_{MB,N^*}(k) + \sum_{M'B'} \int q^2 dq \Gamma^\dagger_{M'B',N^*}(q) G_{M'B'}(q,E) t_{M'B',MB}(q,k;E), \tag{23}$$

with $\Gamma_{MB,N^*}(k)$ being the bare $N^* \to MB$ decay vertex [note that $\Gamma_{N^*,MB}(k) = \Gamma^\dagger_{MB,N^*}(k)$]; the inverse of the dressed N^* propagator is defined by

$$[D^{-1}(E)]_{n,m} = (E - M^0_{N^*_n})\delta_{n,m} - [\Sigma_{N^*}(E)]_{n,m}, \tag{24}$$

where $M^0_{N^*}$ is the mass of the bare N^* and the N^* self-energies $\Sigma_{N^*}(E)$ are given by

$$[\Sigma_{N^*}(E)]_{n,m} \;=\; \sum_{MB} \int_{C_{MB}} k^2 dk \Gamma_{N^*_n,MB}(k) G_{MB}(k;E) \bar{\Gamma}_{MB,N^*_m}(k;E). \tag{25}$$

It is emphasized that the N^* propagator $D(E)$ can have off-diagonal terms. The bare vertex functions in Eqs. (22)-(23) are parametrized as

$$\Gamma_{MB(LS),N^*}(k) \;=\; \frac{1}{(2\pi)^{3/2}} \frac{1}{\sqrt{m_N}} C_{MB(LS),N^*} \left(\frac{\Lambda^2_{MB(LS),N^*}}{\Lambda^2_{MB(LS),N^*} + k^2} \right)^{(2+L/2)} \left(\frac{k}{m_\pi} \right)^L, \tag{26}$$

where L and S denote the orbital angular momentum and spin of the MB state, respectively. This vertex function behaves as k^L at $k \sim 0$ and k^{-4} for $k \to \infty$. The coupling constants $C_{MB(LS),N^*}$, the cutoffs $\Lambda_{MB(LS),N^*}$ and the bare masses $M^0_{N^*}$ are the parameters of the model.

Equations (5)-(25) define the DCC model used in the ANL-Osaka analysis. They are illustrated in Fig. 3. In the absence of theoretical inputs, the DCC model, as well as all

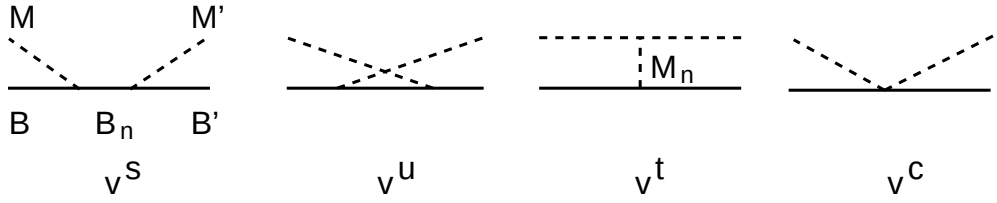

FIG. 1: Meson-exchange mechanisms.

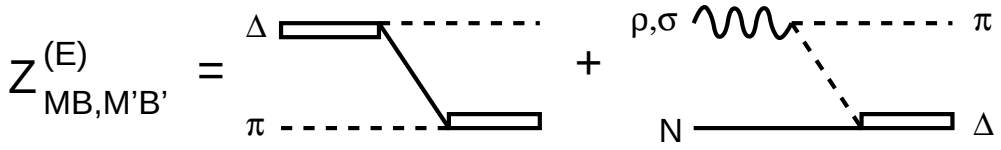

FIG. 2: Z-diagram mechanisms.

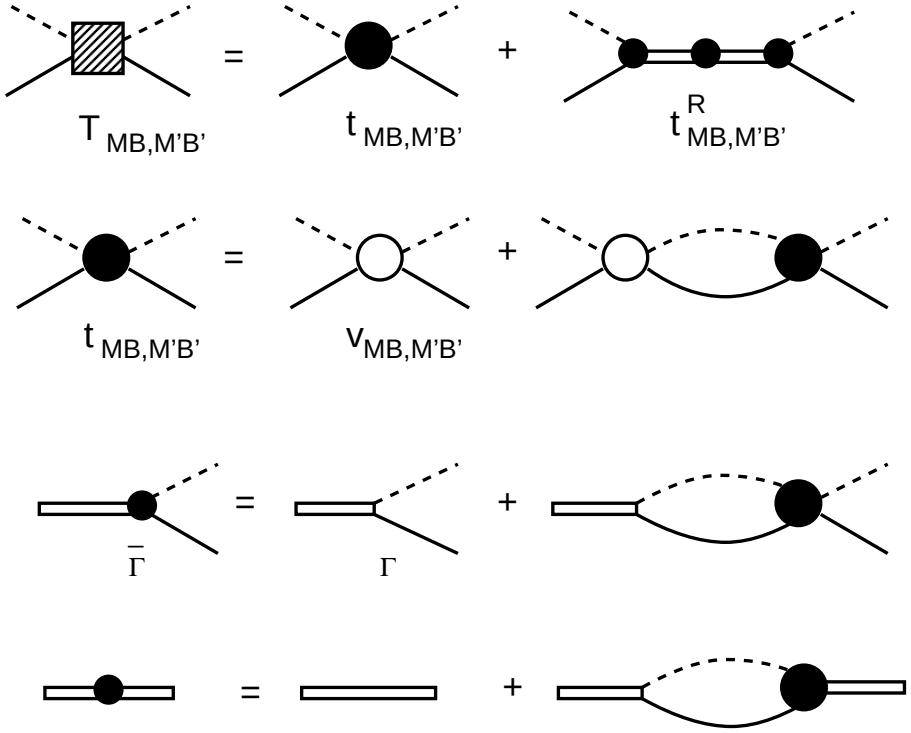

FIG. 3: Graphical representation of Eqs. (5)-(25).

hadron reaction models, has parameters that can only be determined phenomenologically from fitting the data. The meson-exchange interactions $v_{M'B',MB}$ depend on the coupling constants and the cutoffs of form factors that regularize their matrix elements. While the values of some of the coupling constants can be estimated from SU(3) and the previous analysis, we allow most of them to vary in the fits.

B. Electromagnetic amplitudes

With the hadronic amplitudes $t_{M'B',MB}(k',k;E)$ defined in Eq. (6), the partial wave amplitudes for the $\gamma(\vec{q}) + N(-\vec{q}) \to M'(\vec{k}') + B'(-\vec{k})$ reactions are expressed as [4],

$$T_{M'B',\gamma N}(k',q;E) \;=\; t_{M'B',\gamma N}(k',q;E) + t^R_{M'B',\gamma N}(k',q;E), \tag{27}$$

with

$$t_{M'B',\gamma N}(k',q;E) \;=\; v_{M'B',\gamma N}(k',q) + \sum_{M''B''} \int p^2 dp t_{M'B',M''B''}(k',p;E) G_{M''B''}(p;E) v_{M''B'',\gamma N}(p,q), \tag{28}$$

$$t^R_{M'B',\gamma N}(k',q;E) \;=\; \sum_{n,m} \bar{\Gamma}_{M'B',N^*_n}(k';E)[D(E)]_{n,m}\bar{\Gamma}_{N^*_m,\gamma N}(q;E), \tag{29}$$

where the dressed $N^* \to \gamma N$ vertex is

$$\bar{\Gamma}_{N^*,\gamma N}(q;E) \;=\; \Gamma_{N^*,\gamma N}(q) + \sum_{M'B'} \int p^2 dp \Gamma^\dagger_{M'B',N^*}(p) G_{M'B'}(p,E) t_{M'B',\gamma N}(p,q;E). \tag{30}$$

By using Eq.(28), the above equation can be written in terms of dressed $N^* \to MB$ vertex $\bar{\Gamma}_{N^*,M'B'}(p,E)$ defined by Eq.(23)

$$\bar{\Gamma}_{N^*,\gamma N}(q;E) \;=\; \Gamma_{N^*,\gamma N}(q) + \sum_{M'B'} \int p^2 dp \bar{\Gamma}_{N^*,M'B'}(p,E) G_{M'B'}(p,E) v_{M'B',\gamma N}(p,q;E). \tag{31}$$

Here the transition interaction $v_{MB,\gamma N}$ has the tree-diagram mechanisms shown in Fig.1. Thus the pion-loop contributions ($M'B' = \pi N$) to the dressed vertex $\bar{\Gamma}_{N^*,\gamma N}(q;E)$ defined by Eq.(31) can be illustrated in Fig. 4. The procedures for calculating $v_{MB,\gamma N}$ are detailed in Ref. [16].

For the bare $\gamma N \to N^*$ vertex, we write in the helicity representation as

$$\Gamma_{N^*,\gamma N}(q) = \frac{1}{(2\pi)^{3/2}} \sqrt{\frac{m_N}{E_N(q)}} \sqrt{\frac{q_R}{q_0}} G^{N^*}_\lambda(Q^2,q_0) \delta_{\lambda,(\lambda_\gamma - \lambda_N)}, \tag{32}$$

where q_R and q_0 are defined by $M_{N^*} = q_R + E_N(q_R)$ and $W = q_0 + E_N(q_0)$, respectively, and

$$G^{N^*}_\lambda(Q^2,q_0) \;=\; A^{N^*}_\lambda(Q^2,q_0), \qquad \text{for transverse photons,} \tag{33}$$

$$\;=\; S^{N^*}_\lambda(Q^2,q_0), \qquad \text{for longitudinal photons.} \tag{34}$$

The helicity amplitudes $A^{N^*}_\lambda$ and $S^{N^*}_\lambda$ in the above equations are related to the multipole amplitudes $E^{N^*}_{l\pm}, M^{N^*}_{l\pm}, S^{N^*}_{l\pm}$ of $\gamma N \to N^*$ processes. For the N^* of spin $J = l + 1/2$ with l being the orbital angular momentum of the γN system, the helicity amplitudes are

$$A^{N^*}_{3/2}(Q^2,q_0) \;=\; \frac{\sqrt{l(l+2)}}{2}[-M^{N^*}_{l+}(Q^2,q_0) + E^{N^*}_{l+}(Q^2,q_0)], \tag{35}$$

$$A^{N^*}_{1/2}(Q^2,q_0) \;=\; -\frac{1}{2}[lM^{N^*}_{l+}(Q^2,q_0) + (l+2)E^{N^*}_{l+}(Q^2,q_0)], \tag{36}$$

$$S^{N^*}_{1/2}(Q^2,q_0) \;=\; S^{N^*}_{l+}(Q^2,q_0), \tag{37}$$

For N^* with $J = l - 1/2$, we have

$$A^{N^*}_{3/2}(Q^2,q_0) \;=\; -\frac{\sqrt{(l-1)(l+1)}}{2}[M^{N^*}_{l-}(Q^2,q_0) + E^{N^*}_{l-}(Q^2,q_0)], \tag{38}$$

$$A^{N^*}_{1/2}(Q^2,q_0) \;=\; \frac{1}{2}[(l+1)M^{N^*}_{l-}(Q^2,q_0) - (l-1)E^{N^*}_{l-}(Q^2,q_0)], \tag{39}$$

$$S^{N^*}_{1/2}(Q^2,q_0) \;=\; S^{N^*}_{l-}(Q^2,q_0). \tag{40}$$

The multipole amplitudes are parametrized as

$$M^{N^*}_{l\pm}(Q^2,q_0) \;=\; \left(\frac{q_0}{m_\pi}\right)^l \left(\frac{\Lambda^2_{N^*,\gamma N} + m^2_\pi}{\Lambda^2_{N^*,\gamma N} + q^2_0}\right)^{(2+l/2)} \tilde{M}^{N^*}_{l\pm}(Q^2), \tag{41}$$

$$E^{N^*}_{l\pm}(k)(Q^2,q_0) \;=\; \left(\frac{q_0}{m_\pi}\right)^{(l\pm1)} \left(\frac{\Lambda^2_{N^*,\gamma N} + m^2_\pi}{\Lambda^2_{N^*,\gamma N} + q^2_0}\right)^{[2+(l\pm1)/2]} \tilde{E}^{N^*}_{l\pm}(Q^2), \tag{42}$$

$$S^{N^*}_{l\pm}(k)(Q^2,q_0) \;=\; \left(\frac{q_0}{m_\pi}\right)^{(l\pm1)} \left(\frac{\Lambda^2_{N^*,\gamma N} + m^2_\pi}{\Lambda^2_{N^*,\gamma N} + q^2_0}\right)^{[2+(l\pm1)/2]} \tilde{S}^{N^*}_{l\pm}(Q^2), \tag{43}$$

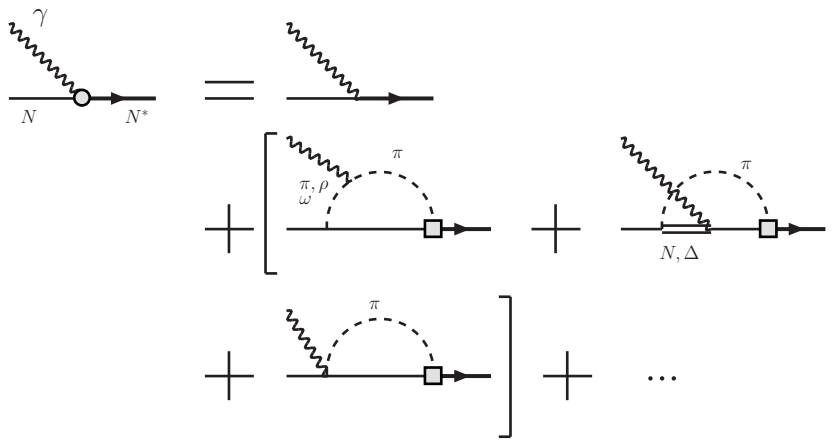

FIG. 4: Dressed $\gamma N \to N^*$ vertex defined by Eq. (32).

where the cutoff $\Lambda_{N^*,\gamma N}$ and the coupling constants $\tilde{M}_{l\pm}(Q^2)$, $\tilde{E}_{l\pm}(Q^2)$, $\tilde{S}_{l\pm}(Q^2)$ are determined in fitting the data. One significant difference between the above parametrization and the form used in our previous analysis [6] is that the multipole amplitudes, or equivalently the helicity amplitudes, for the $\gamma N \to N^*$ processes now have the dependence on the γN relative momentum q_0.

III. EXTRACTIONS OF NUCLEON RESONANCES

We follow the earlier works to define that a nucleon resonance with a complex mass M_R is an "eigenstate" of a Hamiltonian: $H\,|\psi^R_{N^*}\rangle = M_R\,|\psi^R_{N^*}\rangle$. Then from the spectral expansion of the Low Equation for reaction amplitude $T(E) = H' + H'(E-H)^{-1}H'$, where we have defined $H' = H - H_0$ with H_0 being the non-interacting free Hamiltonian, we have

$$T_{MB,M'B'}(k^0_{MB}, k^0_{M'B'}; E \to M_R) \;=\; \frac{\langle k^0_{MB}|\,H'\,|\psi^R_{N^*}\rangle\,\langle\psi^R_{N^*}|\,H'\,|k^0_{M'B'}\rangle}{E - M_R} + \cdot\cdot, \tag{44}$$

where k^0_{MB} and $k^0_{M'B'}$ are the on-shell momenta defined by

$$\begin{aligned} E \;&=\; E_M(k^0_{MB}) + E_B(k^0_{MB}) \\ &=\; E_{M'}(k^0_{M'B'}) + E_{B'}(k^0_{M'B'})\,. \end{aligned} \tag{45}$$

Therefore the resonance positions can also be defined as the poles M_R of the meson-baryon amplitude $T_{MB,M'B'}(k^0_{MB}, k^0_{M'B'}; E)$ on the complex Riemann E-surface. Because of the quadratic relation between the energy and momentum variables, each MB channel for a given E can have a physical (p) sheet characterized by $Im(k^0_{MB}) > 0$ and an unphysical (u) sheet by $Im(k^0_{MB}) < 0$. Like all previous works, we only look for poles close to the physical region and have large effects on πN scattering observables. All of these poles are on the unphysical sheet of the πN channel, but could be on either (u) or (p) sheets of other channels. To find the resonance poles, we analytically continue Eqs. (5)-(25) and Eqs. (28)-(30) to complex E-plane by using the method detailed in Refs. [8, 14]. The main step is to choose appropriate integration paths C_{MB} of Eq. (6) in solving Eqs. (5)-(25).

Explicitly, as energy approaches a resonance position M_R in the complex E-plane, the total meson-baryon amplitudes can be written as

$$T_{MB,M'B'}(k^R_{MB}, k^R_{M'B'}; E \to M_R) \to \frac{\tilde{R}_{MB,M'B'}(M_R)}{E - M_R}\,, \tag{46}$$

with

$$\tilde{R}_{MB,M'B'}(M_R) = \bar{\Gamma}^R_{M'B'}(k^R_{M'B'}, M_R)\bar{\Gamma}^R_{MB}(k^R_{MB}, M_R) \tag{47}$$

where the on-shell momenta $k^R_{MB}, k^R_{M'B'}$ are defined by Eqs. (45) with $E = M_R$. In the actual calculation, the residues $\tilde{R}_{MB,M'B'}(M_R)$ are extracted numerically by using the well known method based on the Cauchy theorem. It is instructive to mention here that for the partial-wave with only one bare N^* state and the resonance can be extracted from $t^R_{M'B',MB}(k', k; E)$ of the full amplitude Eq.(5), each factor of the residue defined by Eq.(47) can be related to the dressed vertex functions Eqs.(22)-(23) and the self energy Eq.(25):

$$\bar{\Gamma}^R_{M'B'}(k^R_{M'B'}, M_R) \;=\; \frac{\bar{\Gamma}_{M'B',N^*}(k^R_{M'B'}, M_R)}{\sqrt{1 - \Sigma'(M_R)}} \tag{48}$$

$$\bar{\Gamma}^R_{MB}(k^R_{MB}, M_R) \;=\; \frac{\bar{\Gamma}_{N^*,MB}(k^R_{MB}, M_R)}{\sqrt{1 - \Sigma'(M_R)}} \tag{49}$$

where $\Sigma'(M_R) = [d\Sigma(E)/dE]_{E=M_R}$.

For the elastic $\pi N \to \pi N$ case, it is customary to define

$$\begin{aligned} R_{\pi N,\pi N}(M_R) \;&=\; \rho_{\pi N}(k^0_{\pi N})\tilde{R}_{\pi N,\pi N}(M_R) \\ &=\; \rho_{\pi N}(k^0_{\pi N})\bar{\Gamma}^R_{\pi N}(k^R_{\pi N}, M_R)\bar{\Gamma}^R_{\pi N}(k^R_{\pi N}, M_R)\,. \end{aligned} \tag{50}$$

where $k^0_{\pi N}$ is defined by $M_R = E_\pi(k^0_{\pi N}) + E_N(k^0_{\pi N})$ and

$$\rho_{\pi N}(k^0_{\pi N}) = \pi\frac{k^0_{\pi N}E_\pi(k^0_{\pi N})E_N(k^0_{\pi N})}{E}. \tag{51}$$

The helicity amplitudes of $\gamma N \to N^*$ at the resonance pole M_R are defined as

$$A_{3/2} \;=\; C \times \bar{\Gamma}^R_{\gamma N}(q_0, M_R, \lambda_\gamma = 1, \lambda_N = -1/2), \tag{52}$$

$$A_{1/2} \;=\; C \times \bar{\Gamma}^R_{\gamma N}(q_0, M_R, \lambda_\gamma = -1, \lambda_N = -1/2)\,, \tag{53}$$

where λ_N and λ_γ are the helicities of the initial nucleon and photon, respectively, and

$$C = \sqrt{\frac{E_N(\vec{q})}{m_N}}\frac{1}{\sqrt{2K}}\sqrt{\frac{(2J^R+1)(2\pi)^3(2q_0)}{4\pi}}, \tag{54}$$

where J^R is the spin of the resonance state, $q_0 = |\vec{q}|$ and $K = (M_R^2 - m_N^2)/(2M_R)$. In practice, we can use the extracted residues $\tilde{R}_{\pi N,\gamma N(\lambda)}$ and $\tilde{R}_{\pi N,\pi N}$ to calculate the determined helicity amplitudes by

$$A_{3/2} \;=\; N \times R_{\pi N\gamma N(3/2)}, \tag{55}$$

$$A_{1/2} \;=\; N \times R_{\pi N\gamma N(1/2)}, \tag{56}$$

$$N = a \times \sqrt{\frac{k^{\rm on}_{\pi N}}{K}\frac{2\pi(2J^R+1)M_R}{m_N R_{\pi N,\pi N}}}, \tag{57}$$

with $a = \sqrt{2/3}$ for the resonance with isospin I=3/2, and $a = -\sqrt{3}$ for I=1/2 resonance; the phase is fixed so that $-\pi/2 \le \arg(N/a) \le \pi/2$.

IV. CALCULATION OF CROSS SECTIONS

A. Meson-baryon scattering

We follow the convention of Goldberger and Watson to define the meson-baryon scattering amplitudes. The normalization of states are : $< \vec{k}|\vec{k}\,' >= \delta(\vec{k}-\vec{k}\,')$ for plane wave states, and $< \phi_\alpha|\phi_\beta >= \delta_{\alpha,\beta}$ for bound states. The T-matrix elements are related to S-matrix elements by

$$S_{MB,M'B'} = \delta_{MB,M'B'} - 2\pi\, i\, \delta(E_{MB} - E_{M'B'})\, T_{MB,M'B'} \tag{58}$$

Note that the " $-$ " sign in the right side of the above equation is opposite to the " $+$ " sign used by the other partial-wave analysis groups such as SAID.

The formula for calculating the meson-baryon scattering cross sections given in this section are in the center of mass system. For the process $M(\vec{k}) + B(-\vec{k}) \to M'(\vec{k}\,') + B'(-\vec{k}\,')$ the differential cross section can be written as

$$\frac{d\sigma_{MB\to M'B'}}{d\Omega_{k'}} \;=\; \frac{(4\pi)^2}{k^2}\rho_{M'B'}(k')\rho_{MB}(k)\frac{1}{(2j_M+1)(2j_B+1)}\sum_{m_{j_M}m_{j_B}}\sum_{m'_{j_M}m'_{j_B}} |< M'B'|t(W)|MB >|^2 \;, \tag{59}$$

where the incoming and outgoing momentum k and k' are defined by the invariant mass W

$$W = E_M(k) + E_B(k) = E_{M'}(k') + E_{B'}(k') \;, \tag{60}$$

where $E_\alpha(k) = \sqrt{m_\alpha^2 + \vec{k}^{\,2}}$ with m_α being the mass of particle α, and the phase-space factor is

$$\rho_{MB}(k) = \pi\frac{kE_M(k)E_B(k)}{W} \;. \tag{61}$$

The scattering amplitude $< M'B'|t(W)|MB >$ in Eq. (59) can be calculated from the partial-wave amplitudes $t^{JT}_{L'S'M'B',LSMB}(k',k,W)$ as

$$\begin{aligned}
&< M'B'|t(W)|MB > \\
&= \sum_{JM_J,T}\;\sum_{L'M'_L,S'M'_S}\;\sum_{LM_L,SM_S} t^{JT}_{L'S'M'B',`LSMB}(k',k,W) \\
&\times[< TM_T|i'_M\tau'_B m'_{i_M}m'_{\tau_B} >< JM_J|L'S'm'_Lm'_S >< S'm'_S|j'_Mj'_Bm'_{j_M}m'_{j_B} > Y^*_{L'm'_L}(\hat{k}\,')] \\
&\times[< TM_T|i_M\tau_B m_{i_M}m_{\tau_B} >< JM_J|LSm_Lm_S >< Sm_S|j_Mj_Bm_{j_M}m_{j_B} > Y_{Lm_L}(\hat{k})] \;,
\end{aligned} \tag{62}$$

where $< jm_j|j_1j_2m_{j_1}m_{j_2} >$ is the Clebsch-Gordon coefficient for the $\vec{j}_1 + \vec{j}_2 = \vec{j}$ coupling, $[(j_Mm_{j_M}),(i_Mm_{i_M})]$ and $[(j_Bm_{j_B}),(\tau_Bm_{\tau_B})]$ are the spin-isospin quantum numbers of mesons and baryons, respectively; $(JM_J)((TM_T))$ are the total angular momentum (total isospin), (LM_L) $((SM_S))$ are the relative orbital angular momentum (total spin) of the considered two-body systems.

By choosing the incoming momentum $\vec{k}$ in the quantization z-component, the total $MB \to M'B'$ cross sections are

$$\sigma^{tot}_{MB\to M'B'}(W) = \int d\Omega_{k'}\frac{d\sigma_{MB\to M'B'}}{d\Omega_{k'}} \;. \tag{63}$$

By optical theorem and the above partial-wave expansion, one can get the $\pi N \to X$ total cross sections averged over the initial spins:

$$\sigma^{tot}_{\pi N\to X}(W) = \frac{-4\pi}{(2s_N+1)k^2}\sum_{J,T,L}(2J+1)\,\rho_{\pi N}(k)\,Im[t^{JT}_{L\frac{1}{2}\pi N,L\frac{1}{2}\pi N}(k,k,W)] \times [< TM_T|1\frac{1}{2}m_{i_\pi}m_{\tau_N}>]^2 \ , \tag{64}$$

where $M_T = m_{i_\pi} + m_{\tau_N}$ and $s_N = 1/2$ is the nucleon spin .

The ANL-Osaka partial-wave amplitudes $t^{JT}_{L'S'M'B',LSMB}(k',k,W)$ can be obtained from the following quantities presented on the webpage:

$$< M'B'|T(W)|MB >= -\rho^{1/2}_{M'B'}(k')t^{JT}_{L'S'M'B',LSMB}(k',k,W)\rho^{1/2}_{MB}(k) \ , \tag{65}$$

for $MB, M'B' = \pi N, \eta N, K\Lambda, K\Sigma$ and $W = W_{th} - 2000$ MeV, where W_{th} is the lower one of the two threshold energies $m_M + m_B$ and $m_{M'} + m_{B'}$. The phase space factors $\rho_{MB}(k)$ and $\rho_{M'B'}(k')$ are defined by Eq.(61).

B. Electro-production of pions

For the pion electroproduction, ($e(p_e)+N(p_N) \to e'(p'_e)+\pi(k)+N(p'_N)$), the differential cross section is conventionally written as

$$\frac{d\sigma}{dE'_e d\Omega_{e'} d\Omega_\pi} \ = \ \Gamma\frac{d\sigma^v}{d\Omega_\pi} \ , \tag{66}$$

where $Q^2 = -q^2$, $q = p_e - p'_e = (\omega_L, \boldsymbol{q}_L)$, $W = \sqrt{(p_N+q)^2}$, and

$$\Gamma \ = \ \frac{\alpha q^\gamma_L}{2\pi^2 Q^2}\frac{E'_e}{E_e}\frac{1}{1-\epsilon}. \tag{67}$$

Here, we have defined $\alpha = e^2/4\pi = 1/137$ and the effective photon energy in the laboratory system and ϵ are given as

$$q^\gamma_L \ = \ \frac{W^2 - m^2_N}{2m_N} \ , \tag{68}$$

$$\epsilon \ = \ [1 + \frac{2\boldsymbol{q}^2_L}{Q^2}\tan^2\frac{\theta_e}{2}]^{-1}, \tag{69}$$

where θ_e is the angle between the outgoing and incoming electrons, and m_N is the nucleon mass and $\boldsymbol{q}_L$ is momentum transfer in the laboratory system.

The differential cross section $d\sigma^v/d\Omega_\pi$ in Eq. (66) is defined in final πN center of mass frame with the following coordinate system:

$$\hat{z} \ = \ \hat{q} = \frac{\boldsymbol{q}}{|\boldsymbol{q}|} \tag{70}$$

$$\hat{y} \ = \ \frac{\boldsymbol{q}\times\boldsymbol{k}}{|\boldsymbol{q}\times\boldsymbol{k}|} \tag{71}$$

$$\hat{x} \ = \ \hat{y}\times\hat{z} \tag{72}$$

We then have the following expression:

$$\frac{d\sigma^v}{d\Omega_\pi} = \frac{d\sigma_T}{d\Omega_\pi} + \epsilon\frac{d\sigma_L}{d\Omega_\pi} + \epsilon\frac{d\sigma_{TT}}{d\Omega_\pi}\cos 2\phi_\pi + \sqrt{2\epsilon(\epsilon+1)}\frac{d\sigma_{LT}}{d\Omega_\pi}\cos\phi_\pi + h_e\sqrt{2\epsilon(1-\epsilon)}\frac{d\sigma_{LT'}}{d\Omega_\pi}\sin\phi_\pi \,, \tag{73}$$

where h_e is the helicity of the incoming electron, ϕ_π is the pion angle measured from the $e-e'$ scattering plane of electron, and

$$\frac{d\sigma_T}{d\Omega_\pi} = \frac{|\boldsymbol{k}|}{|\boldsymbol{q}_\gamma|}\sum_{spin}\frac{F^{xx}+F^{yy}}{2} \,, \tag{74}$$

$$\frac{d\sigma_L}{d\Omega_\pi} = \frac{|\boldsymbol{k}|}{|\boldsymbol{q}_\gamma|}\sum_{spin}\frac{Q^2}{|\boldsymbol{q}|^2}F^{00} \,, \tag{75}$$

$$\frac{d\sigma_{TT}}{d\Omega_\pi} = \frac{|\boldsymbol{k}|}{|\boldsymbol{q}_\gamma|}\sum_{spin}\frac{F^{xx}-F^{yy}}{2} \,, \tag{76}$$

$$\frac{d\sigma_{LT}}{d\Omega_\pi} = \frac{|\boldsymbol{k}|}{|\boldsymbol{q}_\gamma|}\sum_{spin}(-1)\sqrt{\frac{Q^2}{|\boldsymbol{q}|^2}}Re(F^{x0}) \,, \tag{77}$$

$$\frac{d\sigma_{LT'}}{d\Omega_\pi} = \frac{|\boldsymbol{k}|}{|\boldsymbol{q}_\gamma|}\sum_{spin}\sqrt{\frac{Q^2}{|\boldsymbol{q}|^2}}Im(F^{x0}) \,. \tag{78}$$

Here $\boldsymbol{q}$ is the momentum transfer to the initial nucleon and $\boldsymbol{k}$ is the pion momentum in the center of mass system of the final πN state:

$$\omega = \frac{W^2-M_N^2-Q^2}{2W} \,, \tag{79}$$

$$|\boldsymbol{q}| = \sqrt{Q^2+\omega^2} \,, \tag{80}$$

$$|\boldsymbol{k}| = \sqrt{(\frac{W^2+m_\pi^2-M_N^2}{2W})^2 - m_\pi^2} \,, \tag{81}$$

and

$$|\boldsymbol{q}_\gamma| = \frac{W^2-M_N^2}{2W} \,. \tag{82}$$

Here ω and $\boldsymbol{q}_\gamma$ are the energy transfer and the effective photon energy in the center of mass system. Integrating pion angles, Eqs.(66) and (73) lead to

$$\frac{d\sigma}{dE'_e d\Omega_{e'}}(Q^2,W) = \Gamma[\sigma_T(Q^2,W)+\epsilon\sigma_L(Q^2,W)]. \tag{83}$$

where

$$\sigma_{T/L} = \sum_{\pi^+,\pi^0}\int d\Omega_\pi\frac{d\sigma_{T/L}}{d\Omega_\pi} \tag{84}$$

In the coordinate system defined by Eqs.(70)-(72), the pion momentum $\boldsymbol{k}$ is on the $x-z$ plane. We thus can defne

$$\hat{k} \;=\; \boldsymbol{k}/|\boldsymbol{k}| = \cos\theta\hat{z} + \sin\theta\hat{x} \;, \tag{85}$$

where θ is the angle between the outgoing pion and the virtual photon. The quantities F^{ij} with $i,j = x,y,0$ in Eqs. (74)-(78) are defined as

$$\sum_{spin} F^{ij} \;=\; \frac{1}{2}\sum_{m_{s_i},m_{s_f}} < m_{s_f}|\mathcal{F}^i|m_{s_i} >< m_{s_f}|\mathcal{F}^j|m_{s_i} >^* \;, \tag{86}$$

where m_s is the z-component of the nucleon spin, and $\mathcal{F}^i$ is defined by the Chew-Goldberger-Low-Nambu (CGLN) amplitude $\mathcal{F}_{CGLN} = \mathcal{F}^\mu\epsilon_\mu$.

The CGLN amplitude can be expressed in terms of Pauli operator $\boldsymbol{\sigma}$, $\hat{q}$, $\hat{k}$ and the photon polarization vector $\epsilon^\mu = (\epsilon_0, \boldsymbol{\epsilon})$

$$\begin{aligned}\mathcal{F}^\mu\epsilon_\mu = -(&i\boldsymbol{\sigma}\cdot\boldsymbol{\epsilon}_\perp F_1 + \boldsymbol{\sigma}\cdot\hat{k}\boldsymbol{\sigma}\cdot\hat{q}\times\boldsymbol{\epsilon}_\perp F_2 + i\boldsymbol{\sigma}\cdot\hat{q}\hat{k}\cdot\boldsymbol{\epsilon}_\perp F_3 + i\boldsymbol{\sigma}\cdot\hat{k}\hat{k}\cdot\boldsymbol{\epsilon}_\perp F_4 \\ &+i\boldsymbol{\sigma}\cdot\hat{q}\hat{q}\cdot\boldsymbol{\epsilon}F_5 + i\boldsymbol{\sigma}\cdot\hat{k}\hat{q}\cdot\boldsymbol{\epsilon}F_6) + i\boldsymbol{\sigma}\cdot\hat{k}\epsilon_0 F_7 + i\boldsymbol{\sigma}\cdot\hat{q}\epsilon_0 F_8 \,,\end{aligned} \tag{87}$$

where $\boldsymbol{\epsilon}_\perp = \hat{q}\times(\boldsymbol{\epsilon}\times\hat{q})$. By using Eq.(85) and choosing $\epsilon^\mu = (\epsilon_0,\boldsymbol{\epsilon}) = (0,1,0,0),(0,0,1,0),(1,0,0,0)$ to evaluate Eq.(87), we then have

$$\mathcal{F}^x \;=\; i\sigma_x(F_1 - \cos\theta F_2 + \sin^2\theta F_4 + i\sigma_z\sin\theta(F_2 + F_3 + \cos\theta F_4) \;, \tag{88}$$

$$\mathcal{F}^y \;=\; i\sigma_y(F_1 - \cos\theta F_2) - \sin\theta F_2 \;, \tag{89}$$

$$\mathcal{F}^0 \;=\; i\sigma_z(\cos\theta F_7 + F_8) + i\sigma_y\sin\theta F_7 \;. \tag{90}$$

The amplitudes F_i are calculated from the multipole amplitudes $E_{l\pm}, M_{l\pm}, S_{l\pm}$ and $L_{l\pm}$ of the $\gamma^* + N \to \pi N$ process :

$$\begin{aligned}F_1 \;=\; &\sum_l [P'_{l+1}(x)E_{l+}(Q^2,W) + P'_{l-1}(x)E_{l-}(Q^2,W) + lP'_{l+1}(x)M_{l+}(Q^2,W) \\ &+(l+1)P'_{l-1}(x)M_{l-}(Q^2,W)] \,,\end{aligned} \tag{91}$$

$$F_2 \;=\; \sum_l [(l+1)P'_l(x)M_{l+}(Q^2,W) + lP'_l(x)M_{l-}(Q^2,W)] \,, \tag{92}$$

$$\begin{aligned}F_3 \;=\; &\sum_l [P''_{l+1}(x)E_{l+}(Q^2,W) + P''_{l-1}(x)E_{l-}(Q^2,W) - P''_{l+1}(x)M_{l+}(Q^2,W) \\ &+P''_{l-1}(x)M_{l-}(Q^2,W)] \,,\end{aligned} \tag{93}$$

$$F_4 \;=\; \sum_l [-P''_l(x)E_{l+}(Q^2,W) - P''_l(x)E_{l-}(Q^2,W) + P''_l(x)M_{l+}(Q^2,W) - P''_l(x)M_{l-}(Q^2,W)] \,, \tag{94}$$

$$F_5 \;=\; \sum_l [(l+1)P'_{l+1}(x)L_{l+}(Q^2,W) - lP'_{l-1}(x)L_{l-}(Q^2,W)] \,, \tag{95}$$

$$F_6 \;=\; \sum_l [-(l+1)P'_l(x)L_{l+}(Q^2,W) + lP'_l(x)L_{l-}(Q^2,W)] \,, \tag{96}$$

$$F_7 \;=\; \sum_l [-(l+1)P'_l(x)S_{l+}(Q^2,W) + lP'_l(x)S_{l-}(Q^2,W)] \,, \tag{97}$$

$$F_8 \;=\; \sum_l [(l+1)P'_{l+1}(x)S_{l+}(Q^2,W) - lP'_{l-1}(x)S_{l-}(Q^2,W)] \,, \tag{98}$$

where $x = \hat{q} \cdot \hat{k}$, $P_L(x)$ is the Legendre function, $P'_L(x) = dP_L(x)/dx$ and $P''_L(x) = d^2P_L(x)/d^2x$. For the photo-production process $\gamma N \to \pi N$, the differential cross section is $d\sigma_T/d\Omega_\pi$ with $Q^2 = 0$.

The ANL-Osaka multipole amplitudes $E_{l\pm}(Q^2, W)$, $M_{l\pm}(Q^2, W)$, and $L_{l\pm}(Q^2, W)$ for $W = 1080 - 2000$ MeV and $Q^2 = 0 - 3$ (GeV/c)^2 are presented on the webpage.

C. Photo-production of mesons

In the center of mass system, the formula for calculating the un-polarized differential cross section of the photo-production of pseudo-scalar mesons ($M = \pi, \eta, K$) on the nucleon (N), $\gamma(\boldsymbol{q}) + N(-\boldsymbol{q}) \to M(\boldsymbol{k}) + N(-\boldsymbol{k})$, is

$$\frac{d\sigma_0}{d\Omega} = \frac{1}{4} \sum_{m_{s_N}=\pm 1/2} \sum_{m'_{s_N}=\pm 1/2} \sum_{\lambda=\pm 1} \frac{k}{q} | < m'_{s_N} | \mathcal{F}_{CGLN} | m_{s_N} > |^2 \tag{99}$$

where the Chew-Goldberger-Low-Nambu (CGLN) amplitude is defined as

$$\mathcal{F}_{CGLN} = \sum_{i=1,4} O_i F_i(\theta, W) \,. \tag{100}$$

Here we have defined $W = q + E_N(q) = E_M(k) + E_N(k)$, where $E_\alpha(p) = \sqrt{m_\alpha^2 + p^2}$ and m_α is the mass of particle α, and θ is the angle between $\boldsymbol{k}$ and $\boldsymbol{q}$. The operators in the above equation are:

$$\begin{aligned} O_1 &= -i\boldsymbol{\sigma} \cdot \boldsymbol{\epsilon}_\lambda \\ O_2 &= -[\boldsymbol{\sigma} \cdot \hat{k}][\boldsymbol{\sigma} \cdot \hat{q} \times \boldsymbol{\epsilon}_\lambda] \\ O_3 &= -i[\boldsymbol{\sigma} \cdot \hat{q}][\hat{k} \cdot \boldsymbol{\epsilon}_\lambda] \\ O_4 &= -i[\boldsymbol{\sigma} \cdot \hat{k}][\hat{k} \cdot \boldsymbol{\epsilon}_\lambda] \end{aligned}$$

where $\hat{k} = \boldsymbol{k}/|\boldsymbol{k}|$ and $\hat{q} = \boldsymbol{q}/|\boldsymbol{q}| = \hat{z}$, and $\boldsymbol{\sigma}$ is the standard Pauli operator. The quantization direction is chosen to be in the $\hat{z}$-direction, and the photon polarization vectors are $\boldsymbol{\epsilon}_\pm = \frac{\mp}{\sqrt{2}}[\hat{x} \pm i\hat{y}]$. The CGLN amplitudes F_i can be calculated from the multipole anplitudes with $Q^2 = 0$, $E_{l\pm}(W)$ and $M_{l\pm}(W)$, by using Eqs.(91)-(94).

The ANL-Osaka multipole amplitudes $E_{l\pm}(W)$ and $M_{l\pm}(W)$ at $Q^2 = 0$ for $\gamma N \to \pi N, \eta N, \Lambda N, \Sigma N$ and $W = 1080 - 2000$ MeV are presented on the webpage.

The formula for using the multipole amplitudes to calculate the polarization observables can be found in Ref.[15].

D. Inclusive $N(e, e')$ cross sections

For the inclusive process, $e(p_e) + N(p_N) \to e'(p'_e) + X$, the differential cross section is written by using structure functions W_i as

$$\frac{d\sigma}{dE'_e d\Omega_{e'}}(Q^2, W) = \frac{\alpha^2}{4E_e^2 \sin^4 \frac{\theta_e}{2}} [W_2(Q^2, W) \cos^2 \frac{\theta_e}{2} + 2W_1(Q^2, W) \sin^2 \frac{\theta_e}{2}] \tag{101}$$

The structure functions are defined from the hadron tensor $W^{\mu\nu}$ as

$$W^{\mu\nu} = \sum_{\bar{i}} \sum_{f} (2\pi)^3 \delta^4(P+q-P') \frac{E_N(P)}{m_N} < f(P')|J^{\mu}_{em}|N(P) >< f(P')|J^{\nu}_{em}|N(P) >^*$$
$$= (-g^{\mu\nu} + \frac{q^\mu q^\nu}{q^2}) W_1(Q^2, W) + \frac{W_2(Q^2, W)}{m_N^2} \hat{P}^\mu \hat{P}^\nu, \quad (102)$$

where $\hat{P}^\mu = P^\mu - q^\mu (P \cdot q)/q^2$.

The structure functions are also expressed by virtual photon cross sections σ_T^X and σ_L^X as

$$W_1(Q^2, W) = \frac{q_L^\gamma}{4\pi^2 \alpha} \sigma_T^X(Q^2, W) \quad (103)$$
$$W_2(Q^2, W) = \frac{q_L^\gamma}{4\pi^2 \alpha} \frac{Q^2}{\boldsymbol{q}_L^2} [\sigma_T^X(Q^2, W) + \sigma_L^X(Q^2, W)]. \quad (104)$$

The inclusive cross section can then be written as

$$\frac{d\sigma}{dE'_e d\Omega_{e'}}(Q^2, W) = \Gamma[\sigma_T^X(Q^2, W) + \epsilon \sigma_L^X(Q^2, W)]. \quad (105)$$

where ϵ is defined in Eq.(69). If only the single pion contribution to W_1 and W_2 is kept in evaluating Eq.(102), $\sigma^X_{T/L}$ will be identical to $\sigma_{T/L}$ defined in Eq.(83).

The ANL-Osaka structure functions $W_1(Q^2, W)$ and $W_2(Q^2, W)$ for $Q^2 = 0 - 3(\mathrm{GeV/c})^2$ and $W = 1080 - 2000$ MeV are presented on the webpage.

E. $\pi N \to \pi\pi N$ cross sections

In the center of mass frame, the momentum variables of the $\pi N \to \pi\pi N$ reaction with invariant mass W can be specified as

$$a(\vec{p}_a) + b(\vec{p}_b) \to c(\vec{p}_c) + d(\vec{p}_d) + e(\vec{p}_e) \ , \quad (106)$$

where $\vec{p}_a = -\vec{p}_b = \vec{k}$ with k defined by $W = E_a(k) + E_b(k)$, $\vec{p}_c + \vec{p}_d = -\vec{p}_e = \vec{k'}$, and $(c+d+e)$ can be any possible charged states formed from two pions and one nucleon. The total cross section of the process Eq. (106) can be written as

$$\sigma^{rec}_{ab\to cde} = \int_{m_c+m_d}^{W-m_e} \frac{d\sigma^{rec}}{dM_{cd}} dM_{cd} \ , \quad (107)$$

with

$$\frac{d\sigma^{rec}}{dM_{cd}} = \frac{\rho_i}{k^2} 16\pi^3 \int d\Omega_{k_{cd}} d\Omega_{k'} \frac{k_{cd} k'}{W} \frac{1}{(2s_a+1)(2s_b+1)} \sum_{i,f} |\sqrt{E_c E_d E_e} \langle \vec{p}_c \vec{p}_d \vec{p}_e, f|T|\vec{k}, i\rangle|^2 \ , \quad (108)$$

where $\rho_i = \pi \frac{kE_a(k)E_b(k)}{W}$,$i, f$ denote all spin (s_a, s_{az}) and isospin (t_a, t_{az}) quantum numbers, and $\sum_{i,f}$ means summing over only spin quantum numbers. For a given invariant mass M_{cd},

$\vec{k}_{cd}$ is the relative momentum between c and d in the center of mass of the sub-system (cd) . It follows that k' and k_{cd} are defined by W and M_{cd}:

$$\begin{aligned} M_{cd} &= E_c(k_{cd}) + E_d(k_{cd})\,, \\ W &= E_e(k') + E_{cd}(k')\,, \\ E_{cd}(k') &= \sqrt{M_{cd}^2 + (k')^2}\,. \end{aligned} \tag{109}$$

The T-matrix elements in the Eq. (108) are of the following form

$$\begin{aligned} \langle \vec{p}_c \vec{p}_d \vec{p}_e, f|T|\vec{k}, i\rangle &= \sum_{s_{R_z}, t_{R_z}} \frac{\langle \vec{p}_c, s_{cz}, t_{cz}; \vec{p}_d, s_{dz}, t_{dz}|H_I|\vec{k}', s_{Rz}, t_{R_z}\rangle}{W - E_e(k') - E_R(k') - \Sigma_{eR}(k', E)} \\ &\quad \times \langle \vec{k}', s_{Rz}, t_{Rz}; -\vec{k}', s_{ez}, t_{ez}|T|\vec{k}, s_{az}, t_{az}; -\vec{k}, s_{bz}, t_{bz}\rangle\ , \end{aligned} \tag{110}$$

where R is a bare state which has $R \to cd$ decay channel. For the $eR = \pi\Delta$ and $eR = \rho N$ channels, the self-energies are explicitly given by

$$\Sigma_{\pi\Delta}(k; W) = \frac{m_\Delta}{E_\Delta(k)} \int q^2 dq \frac{M_{\pi N}(q)}{[M_{\pi N}^2(q) + k^2]^{1/2}} \frac{|f_{\Delta\to\pi N}(q)|^2}{W - E_\pi(k) - [M_{\pi N}^2(q) + k^2]^{1/2} + i\epsilon}, \tag{111}$$

$$\Sigma_{\rho N}(k; W) = \frac{m_\rho}{E_\rho(k)} \int q^2 dq \frac{M_{\pi\pi}(q)}{[M_{\pi\pi}^2(q) + k^2]^{1/2}} \frac{|f_{\rho\to\pi\pi}(q)|^2}{W - E_N(k) - [M_{\pi\pi}^2(q) + k^2]^{1/2} + i\epsilon}, \tag{112}$$

where $m_\Delta = 1280$ MeV, $m_\rho = 812$ MeV, $M_{\pi N}(q) = E_\pi(q) + E_N(q)$, and $M_{\pi\pi}(q) = E_\pi(q) + E_\pi(q)$. The form factors $f_{\Delta\to\pi N}(q)$ and $f_{\rho\to\pi\pi}(q)$ are for describing the $\Delta \to \pi N$ and $\rho \to \pi\pi$ decays in the Δ and ρ rest frames, respectively. They are parametrized as:

$$f_{\Delta\to\pi N}(q) = -i\frac{(0.98)}{[2(m_N + m_\pi)]^{1/2}} \left(\frac{q}{m_\pi}\right) \left(\frac{1}{1 + [q/(358\ \text{MeV})]^2}\right)^2, \tag{113}$$

$$f_{\rho\to\pi\pi}(q) = \frac{(0.6684)}{\sqrt{m_\pi}} \left(\frac{q}{(461\ \text{MeV})}\right) \left(\frac{1}{1 + [q/(461\ \text{MeV})]^2}\right)^2. \tag{114}$$

The σ self-energy $\Sigma_{\sigma N}(k; E)$ is calculated from a $\pi\pi$ s-wave scattering model with a vertex function $g(q)$ for the $\sigma \to \pi\pi$ decay and a separable interaction $v(q', q) = h_0 h(q') h(q)$. The resulting form is

$$\Sigma_{\sigma N}(k; W) = \langle g G_{\pi\pi} g\rangle(k; W) + \tau(k; E)[\langle g G_{\pi\pi} h\rangle(k; W)]^2, \tag{115}$$

with

$$\tau(k; W) = \frac{h_0}{1 - h_0\langle h G_{\pi\pi} h\rangle(k; W)}, \tag{116}$$

$$\begin{aligned} \langle h G_{\pi\pi} h\rangle(k; W) &= \int dq q^2 \frac{M_{\pi\pi}(q)}{[M_{\pi\pi}^2(q) + k^2]^{1/2}} \\ &\quad \times \frac{h(q)^2}{W - E_N(k) - [M_{\pi\pi}^2(q) + k^2]^{1/2} + i\varepsilon}, \end{aligned} \tag{117}$$

$$\langle g G_{\pi\pi} g\rangle(k; W) = \frac{m_\sigma}{E_\sigma(k)} \int dq q^2 \frac{M_{\pi\pi}(q)}{[M_{\pi\pi}^2(q) + k^2]^{1/2}}$$

$$\times \frac{g(q)^2}{W - E_N(k) - [M^2_{\pi\pi}(q) + k^2]^{1/2} + i\varepsilon}, \tag{118}$$

$$\langle gG_{\pi\pi}h\rangle(k;W) = \sqrt{\frac{m_\sigma}{E_\sigma(k)}} \int dq q^2 \frac{M_{\pi\pi}(q)}{[M^2_{\pi\pi}(q) + k^2]^{1/2}} \times \frac{g(q)h(q)}{W - E_N(k) - [M^2_{\pi\pi}(q) + k^2]^{1/2} + i\varepsilon}. \tag{119}$$

In the above equations, $m_\sigma = 700.0$ MeV and the form factors are

$$g(p) = \frac{g_0}{\sqrt{m_\pi}} \frac{1}{1 + (cp)^2}, \tag{120}$$

$$h(p) = \frac{1}{m_\pi} \frac{1}{1 + (dp)^2}. \tag{121}$$

where $g_0 = 1.638$, $h_0 = 0.556$, $c = 1.02$ fm, and $d = 0.514$ fm.

For any spins and isospins and c.m. momenta $\vec{p}$ and $\vec{p}^{'}$, the $MB \to M'B'$ T-matrix elements in Eq.(110) are in general defined by

$$\begin{aligned}
&\langle \vec{p}^{'}, s_{M'z}, t_{M'z}; -\vec{p}^{'}, s_{B'z}, t_{B'z}|T|\vec{p}, s_{Mz}, t_{Mz}; -\vec{p}, s_{Bz}, t_{Bz}\rangle \\
&= \sum_{JM,TT_z} \sum_{L'M'_L,S'S'_z} \sum_{LM_L,SS_z} Y_{L',M'_L}(\hat{p}')Y^*_{L,M_L}(\hat{p}) \\
&\times \langle s_{M'}, s_{B'}, s_{M'z}, s_{B'z}|S', S'_z\rangle\langle L', S', M'_L, S'_z|J, M\rangle\langle t_{M'}, t_{B'}, t_{M'z}, t_{B'z}|T, T_z\rangle \\
&\times \langle s_M, s_B, s_{Mz}, s_{Bz}|S, S_z\rangle\langle L, S, M_L, S_z|J, M\rangle\langle t_M, t_B, t_{Mz}, t_{Bz}|T, T_z\rangle \\
&\times t^{JT}_{L'S'M'B',LSMB}(p', p, W),
\end{aligned} \tag{122}$$

where the matrix elements $t^{JT}_{L'S'M'B',LS\pi N}(p', p, W)$ for $M'B' = \pi\Delta, \sigma N, \rho N$ are the PWA from the ANL-Osaka model.

The matrix elements of H_I of Eq. (110) describe the decay of a resonance $R = \Delta, \rho, \sigma$ into a two-particle state cd. It is of the following expression

$$\begin{aligned}
&\langle \vec{p}_c, s_{cz}, t_{cz}; \vec{p}_d, s_{dz}, t_{dz}|H_I|\vec{k}', s_{Rz}, t_{Rz}\rangle \\
&= \delta(\vec{p}_c + \vec{p}_d - \vec{k}') \sqrt{\frac{E_c(k_{cd})E_d(k_{cd})M_R}{E_c(p_c)E_d(p_d)E_R(k')}} \langle \vec{k}_{cd}, s_{cz}, t_{cz}; -\vec{k}_{cd}, s_{dz}, t_{dz}|H_I|\vec{0}, s_{Rz}, t_{Rz}\rangle,
\end{aligned} \tag{123}$$

with

$$\begin{aligned}
&\langle \vec{k}_{cd}, s_{cz}, t_{cz}; -\vec{k}_{cd}, s_{dz}, t_{dz}|H_I|\vec{0}, s_{Rz}, t_{Rz}\rangle \\
&= \sum_{L_{cd},S_{cd},m_{cd},S_{cdz}} [\langle s_c, s_d, s_{cz}, s_{dz}|S_{cd}, S_{cdz}\rangle\langle L_{cd}, S_{cd}, m_{cd}, S_{cdz}|s_R, s_{Rz}\rangle \\
&\quad \times \langle t_c, t_d, t_{cz}, t_{dz}|t_R, t_{Rz}\rangle Y_{L_{cd},m_{cd}}(\hat{k}_{cd})F_{L^R_{cd},S^R_{cd}}(k_{cd})]\delta_{L_{cd},L^R_{cd}}\delta_{S_{cd},S^R_{cd}} .
\end{aligned} \tag{124}$$

The vertex functions are

$$F_{L^\Delta_{\pi N},S^\Delta_{\pi N}}(q) = if_{\Delta\to\pi N}(q) , \tag{125}$$

$$F_{L^\sigma_{\pi\pi},S^\sigma_{\pi\pi}}(q) = \sqrt{2}g(q) , \tag{126}$$

$$F_{L^\rho_{\pi\pi},S^\rho_{\pi\pi}}(q) = (-1)\sqrt{2}f_{\rho\to\pi\pi}(q) , \tag{127}$$

where $L^{\Delta}_{\pi N}=1, S^{\Delta}_{\pi N}=3/2$, $L^{\sigma}_{\pi\pi}=0, S^{\sigma}_{\pi\pi}=0$, $L^{\rho}_{\pi\pi}=1, S^{\rho}_{\pi\pi}=1$. Here it is noted that the factor $\sqrt{2}$ in Eqs. (126)-(127) comes from the Bose symmetry of pions, and the phase factor i and (-1) are chosen to be consistent with the non-resonant interactions involving $\pi N\Delta$, $\sigma\pi\pi$ and $\rho\pi\pi$ vertex interactions. The form factors $f_{\Delta\to\pi N}(q)$ and $f_{\rho\to\pi\pi}(q)$ have been in Eqs.(113)-(114) and $g(q)$ in Eq.(120).

With the above equations, the contribution from $\pi N\to\pi\Delta\to\pi\pi N$ to the total cross section $\sigma^{rec}_{\pi N\to\pi\pi N}$, as defined by Eq. (107)-(108), can be written as

$$\sigma^{rec}_{\pi\Delta}(W) \;=\; \int_{m_N+m_\pi}^{W-m_\pi} dM_{\pi N}\frac{M_{\pi N}}{E_\Delta(k)}\frac{\Gamma_\Delta/(2\pi)}{|W-E_\pi(k)-E_\Delta(k)-\Sigma_{\pi\Delta}(k,W)|^2}\times\sigma_{\pi N\to\pi\Delta}\;, \tag{128}$$

where k and $E_\Delta(k)$ are defined by W and $M_{\pi N}$

$$k \;=\; \frac{1}{2W}[(W^2-M^2_{\pi N}-m^2_\pi)^2-4M^2_{\pi N}m^2_\pi]^{1/2}\,, \tag{129}$$

$$E_\Delta(k) \;=\; [m^2_\Delta+k^2]^{1/2}\,, \tag{130}$$

$\Sigma_{\pi\Delta}(k,W)$is defined in Eq. (111), $\Gamma_\Delta=-2Im[\Sigma_{\pi\Delta}(k=0,W)]$, and

$$\begin{aligned}\sigma_{\pi N\to\pi\Delta} \;=\; &\frac{4\pi}{k_0^2}\sum_{JT,L'S',LS}\frac{2J+1}{(2S_N+1)(2S_\pi+1)}|\rho^{1/2}_{\pi\Delta}(k)t^{JT}_{L'S'\pi\Delta,LS\pi N}(k,k_0;W)\rho^{1/2}_{\pi N}(k_0)|^2\\ &\times\langle t_\pi,t_N,t^z_\pi,t^z_N|T,T^z\rangle^2\;,\end{aligned} \tag{131}$$

where k_0 is defined by $W=E_\pi(k_0)+E_N(k_0)$ and $\rho_{ab}(k)=\pi kE_a(k)E_b(k)/W$. Similarly, the contributions of $\pi N\to\rho N\to\pi\pi N$ and $\pi N\to\sigma N\to\pi\pi N$ to the total cross section $\sigma^{rec}_{\pi N\to\pi\pi N}$ are

$$\sigma^{rec}_{aN}(W) \;=\; \int_{2m_\pi}^{W-m_N} dM_{\pi\pi}\frac{M_{\pi\pi}}{E_a(k)}\frac{\Gamma_a/(2\pi)}{|W-E_N(k)-E_a(k)-\Sigma_{aN}(k,W)|^2}\times\sigma_{\pi N\to aN}\;, \tag{132}$$

where $a=\rho,\sigma$, k is defined by $M_{\pi\pi}$ and W

$$k \;=\; \frac{1}{2W}[(W^2-M^2_{\pi\pi}-m^2_N)^2-4M^2_{\pi\pi}m^2_N]^{1/2}\,, \tag{133}$$

$$E_a(k) \;=\; [m^2_a+k^2]^{1/2}\,, \tag{134}$$

$\Sigma_{aN}(k,W)$ for $aN=\rho N,\sigma N$ are is defined in Eqs.(104) and (107), $\Gamma_a=-2Im[\Sigma_{aN}(k=0,W)]$, and

$$\begin{aligned}\sigma_{\pi N\to aN} \;=\; &\frac{4\pi}{k_0^2}\sum_{JT,L'S',LS}\frac{2J+1}{(2S_N+1)(2S_\pi+1)}|\rho^{1/2}_{aN}(k)t^{JT}_{L'S'aN,LS\pi N}(k,k_0;W)\rho^{1/2}_{\pi N}(k_0)|^2\\ &\times\langle t_\pi,t_N,t^z_\pi,t^z_N|T,T^z\rangle^2\;.\end{aligned} \tag{135}$$

To perform calculations, we need to have the partial-wave amplitudes $t^{JT}_{L'S'M'B',LS\pi N}(p,k,W)$ for $M'B'=\pi\Delta,\rho N,\sigma N$. These PWA from ANL-Osaka model can be obtained from the webpage which present the following :

$$\begin{aligned}<\pi\Delta|T(W)|\pi N> &= -\rho^{1/2}_{\pi\Delta}(p_\Delta)t^{JT}_{L'S'\pi\Delta,LS\pi N}(p_\Delta,k,W)\rho^{1/2}_{\pi N}(k)\;,\\ <\rho N|T(W)|\pi N> &= -\rho^{1/2}_{\rho N}(p_\rho)t^{JT}_{L'S'\rho N,LS\pi N}(p_\rho,k,W)\rho^{1/2}_{\pi N}(k)\;,\\ <\sigma N|T(W)|\pi N> &= -\rho^{1/2}_{\sigma N}(p_\sigma)t^{JT}_{L'S'\sigma N,LS\pi N}(p_\sigma,k,W)\rho^{1/2}_{\pi N}(k)\;,\end{aligned} \tag{136}$$

Here the phase space factors account for the effects due to $\Delta \to \pi N$, $\sigma \to \pi\pi$ and $\rho \to \pi\pi$ decays. Explicitly, we have

$$\rho_{\pi\Delta}(p_\Delta) \;=\; \pi \frac{p_\Delta E_\Delta(p_\Delta) E_\pi(p_\Delta)}{W} \;, \tag{137}$$

where p_Δ and $E_\Delta(p_\Delta)$ are defined by W and the invariant mass $M_{\pi N}$ in the integrations of Eqs.(107) and (128)

$$p_\Delta \;=\; \frac{1}{2W}[(W^2 - M_{\pi N}^2 - m_\pi^2)^2 - 4M_{\pi N}^2 m_\pi^2]^{1/2} \,, \tag{138}$$

$$E_\Delta(p_\Delta) \;=\; [M_{\pi N}^2 + p_\Delta^2]^{1/2} \,, \tag{139}$$

For the calculations of Eqs.(107) and (128), we thus present $< \pi\Delta|T(W)|\pi N >$ in the range $0 \le p_\Delta \le p_{\Delta,max}$ with

$$p_{\Delta,max} = \frac{1}{2W}[(W^2 - (m_\pi + m_N)^2 - m_\pi^2)^2 - 4(m_\pi + m_N)^2 m_\pi^2]^{1/2} \;. \tag{140}$$

For the ρN and σN channels, we have

$$\rho_{\sigma N}^{1/2}(p_\sigma) \;=\; \pi \frac{p_\sigma E_\sigma(p_\sigma) E_N(p_\sigma)}{W} \;, \tag{141}$$

$$\rho_{\rho N}^{1/2}(p_\rho) \;=\; \pi \frac{p_\rho E_\rho(p_\rho) E_N(p_\rho)}{W} \;, \tag{142}$$

For $a = \sigma$ and ρ, we have

$$p_a \;=\; \frac{1}{2W}[(W^2 - M_{\pi\pi}^2 - m_N^2)^2 - 4M_{\pi\pi}^2 m_N^2]^{1/2} \,, \tag{143}$$

$$E_a(p_a) \;=\; [M_{\pi\pi}^2 + p_a^2]^{1/2} \,. \tag{144}$$

For the calculation of Eqs.(107) and (132), we thus present $< \rho N|T(W)|\pi N >$ and $< \sigma N|T(W)|\pi N >$ in the range $0 \le p_a \le p_{a,max}$ with

$$p_{a,max} = \frac{1}{2W}[(W^2 - (2m_\pi)^2 - m_N^2)^2 - 4(2m_\pi)^2 m_N^2]^{1/2} \;. \tag{145}$$

The above equations are for the calculations of the $\pi N \to \pi\pi N$ through the resonant $\pi\Delta$, σN and ρN channels. There are also weaker contributions from the direct production mechanisms, as illustrated in Fig. 5, which can be calculated by using the procedures explained in Ref. [11].

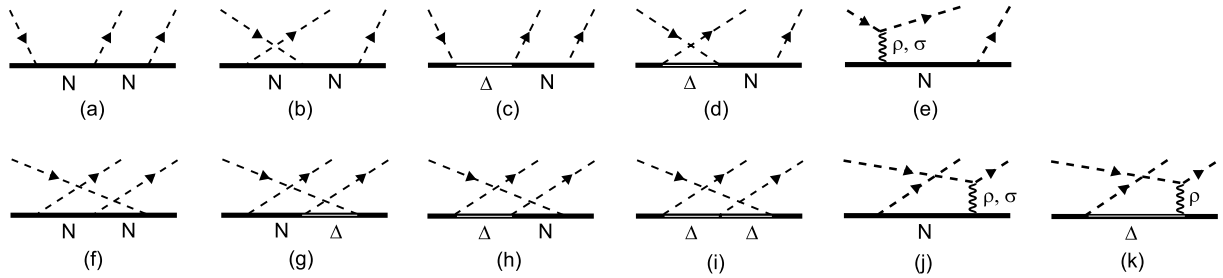

FIG. 5: The considered $v_{\pi N,\pi\pi N}$.

V. DATA

The parameters of the ANL-Osaka DCC model were determined by performing χ^2-fits to the data of $\pi N, \gamma N \to \pi N, \eta N, K\Lambda, K\Sigma$. The calculations involve solving the coupled-channel Eqs. (5)-(25). The meson-baryon partial-waves included in the calculations are listed in Table I. The total number of the data included in the fits are about 30,000 data points, as listed in table II-V.

Note that the 1940 data points for $\pi N \to \pi N$ listed in Table II are in fact contain information of about 30,000 data in the SAID analysis : 14196 of $\pi^+ p \to \pi^+ p$, 13895 of $\pi^- p \to \pi^- p$, and 2877 of $\pi^- p \to \pi^0 n$. In addition, the partial-wave amplitudes of $\pi N \to \pi\pi N$ determined from the very extensive bubble-chamber data of $\pi N \to \pi\pi N$ were also used in the earlier analysis of SAID. Thus the determined PWA for $\pi N \to \pi N, \pi\Delta, \rho N, \sigma N$ are rather reliable.

On the other hand, the data points for $\pi N \to \eta N, K\Lambda, K\Sigma$ listed in Table III are much less, only 294, 941, and 1262, respectively. Thus the determined PWA for these processes need to be improved by using more extensive data which could be available from experiments at J-PARC in near future.

In Tables IV and V, we see that the data points for $\gamma N \to \pi N$ are much more than those of $\gamma N \to \eta N, K\Lambda, K\Sigma$. Therefore, the $\gamma N \to N^*$ couplings are mainly determined by the predicted multipole amplitudes of $\gamma N \to \pi N$. It will be interesting to include more new JLab data of $\gamma N \to K\Lambda, K\Sigma$ in the analysis to further improve the determination of $\gamma N \to N^*$ couplings which are crucial to test the predictions from LQCD and various hadron models.

TABLE I: The orbital angular momentum (L) and total spin (S) of each MB channel allowed in a given partial wave. In the first column, partial waves are denoted with the conventional notation l_{2I2J} as well as (I,J^P).

l_{2I2J} (I,J^P)	(L,S) of the considered partial waves									
	πN	ηN	$\pi\Delta$		σN	ρN			$K\Lambda$	$K\Sigma$
			$(\pi\Delta)_1$	$(\pi\Delta)_2$		$(\rho N)_1$	$(\rho N)_2$	$(\rho N)_3$		
S_{11} $(1,\frac{1}{2}^-)$	$(0,\frac{1}{2})$	$(0,\frac{1}{2})$	$(2,\frac{3}{2})$	–	$(1,\frac{1}{2})$	$(0,\frac{1}{2})$	$(2,\frac{3}{2})$	–	$(0,\frac{1}{2})$	$(0,\frac{1}{2})$
S_{31} $(3,\frac{1}{2}^-)$	$(0,\frac{1}{2})$	–	$(2,\frac{3}{2})$	–	–	$(0,\frac{1}{2})$	$(2,\frac{3}{2})$	–	–	$(0,\frac{1}{2})$
P_{11} $(1,\frac{1}{2}^+)$	$(1,\frac{1}{2})$	$(1,\frac{1}{2})$	$(1,\frac{3}{2})$	–	$(0,\frac{1}{2})$	$(1,\frac{1}{2})$	$(1,\frac{3}{2})$	–	$(1,\frac{1}{2})$	$(1,\frac{1}{2})$
P_{13} $(1,\frac{3}{2}^+)$	$(1,\frac{1}{2})$	$(1,\frac{1}{2})$	$(1,\frac{3}{2})$	$(3,\frac{3}{2})$	$(2,\frac{1}{2})$	$(1,\frac{1}{2})$	$(1,\frac{3}{2})$	$(3,\frac{3}{2})$	$(1,\frac{1}{2})$	$(1,\frac{1}{2})$
P_{31} $(3,\frac{1}{2}^+)$	$(1,\frac{1}{2})$	–	$(1,\frac{3}{2})$	–	–	$(1,\frac{1}{2})$	$(1,\frac{3}{2})$	–	–	$(1,\frac{1}{2})$
P_{33} $(3,\frac{3}{2}^+)$	$(1,\frac{1}{2})$	–	$(1,\frac{3}{2})$	$(3,\frac{3}{2})$	–	$(1,\frac{1}{2})$	$(1,\frac{3}{2})$	$(3,\frac{3}{2})$	–	$(1,\frac{1}{2})$
D_{13} $(1,\frac{3}{2}^-)$	$(2,\frac{1}{2})$	$(2,\frac{1}{2})$	$(0,\frac{3}{2})$	$(2,\frac{3}{2})$	$(1,\frac{1}{2})$	$(2,\frac{1}{2})$	$(0,\frac{3}{2})$	$(4,\frac{3}{2})$	$(2,\frac{1}{2})$	$(2,\frac{1}{2})$
D_{15} $(1,\frac{5}{2}^-)$	$(2,\frac{1}{2})$	$(2,\frac{1}{2})$	$(2,\frac{3}{2})$	$(4,\frac{3}{2})$	$(3,\frac{1}{2})$	$(2,\frac{1}{2})$	$(2,\frac{3}{2})$	$(4,\frac{3}{2})$	$(2,\frac{1}{2})$	$(2,\frac{1}{2})$
D_{33} $(3,\frac{3}{2}^-)$	$(2,\frac{1}{2})$	–	$(0,\frac{3}{2})$	$(2,\frac{3}{2})$	–	$(2,\frac{1}{2})$	$(0,\frac{3}{2})$	$(2,\frac{3}{2})$	–	$(2,\frac{1}{2})$
D_{35} $(3,\frac{5}{2}^-)$	$(2,\frac{1}{2})$	–	$(2,\frac{3}{2})$	$(4,\frac{3}{2})$	–	$(2,\frac{1}{2})$	$(2,\frac{3}{2})$	$(4,\frac{3}{2})$	–	$(2,\frac{1}{2})$
F_{15} $(1,\frac{5}{2}^+)$	$(3,\frac{1}{2})$	$(3,\frac{1}{2})$	$(1,\frac{3}{2})$	$(3,\frac{3}{2})$	$(2,\frac{1}{2})$	$(3,\frac{1}{2})$	$(1,\frac{3}{2})$	$(3,\frac{3}{2})$	$(3,\frac{1}{2})$	$(3,\frac{1}{2})$
F_{17} $(1,\frac{7}{2}^+)$	$(3,\frac{1}{2})$	$(3,\frac{1}{2})$	$(3,\frac{3}{2})$	$(5,\frac{3}{2})$	$(4,\frac{1}{2})$	$(3,\frac{1}{2})$	$(3,\frac{3}{2})$	$(5,\frac{3}{2})$	$(3,\frac{1}{2})$	$(3,\frac{1}{2})$
F_{35} $(3,\frac{5}{2}^+)$	$(3,\frac{1}{2})$	–	$(1,\frac{3}{2})$	$(3,\frac{3}{2})$	–	$(3,\frac{1}{2})$	$(1,\frac{3}{2})$	$(3,\frac{3}{2})$	–	$(3,\frac{1}{2})$
F_{37} $(3,\frac{7}{2}^+)$	$(3,\frac{1}{2})$	–	$(3,\frac{3}{2})$	$(5,\frac{3}{2})$	–	$(3,\frac{1}{2})$	$(3,\frac{3}{2})$	$(5,\frac{3}{2})$	–	$(3,\frac{1}{2})$
G_{17} $(1,\frac{7}{2}^-)$	$(4,\frac{1}{2})$	$(4,\frac{1}{2})$	$(2,\frac{3}{2})$	$(4,\frac{3}{2})$	$(3,\frac{1}{2})$	$(4,\frac{1}{2})$	$(2,\frac{3}{2})$	$(4,\frac{3}{2})$	$(4,\frac{1}{2})$	$(4,\frac{1}{2})$
G_{19} $(1,\frac{9}{2}^-)$	$(4,\frac{1}{2})$	$(4,\frac{1}{2})$	$(4,\frac{3}{2})$	$(6,\frac{3}{2})$	$(5,\frac{1}{2})$	$(4,\frac{1}{2})$	$(4,\frac{3}{2})$	$(6,\frac{3}{2})$	$(4,\frac{1}{2})$	$(4,\frac{1}{2})$
G_{37} $(3,\frac{7}{2}^-)$	$(4,\frac{1}{2})$	–	$(2,\frac{3}{2})$	$(4,\frac{3}{2})$	–	$(4,\frac{1}{2})$	$(2,\frac{3}{2})$	$(4,\frac{3}{2})$	–	$(4,\frac{1}{2})$
G_{39} $(3,\frac{9}{2}^-)$	$(4,\frac{1}{2})$	–	$(4,\frac{3}{2})$	$(6,\frac{3}{2})$	–	$(4,\frac{1}{2})$	$(4,\frac{3}{2})$	$(6,\frac{3}{2})$	–	$(4,\frac{1}{2})$
H_{19} $(1,\frac{9}{2}^+)$	$(5,\frac{1}{2})$	$(5,\frac{1}{2})$	$(3,\frac{3}{2})$	$(5,\frac{3}{2})$	$(4,\frac{1}{2})$	$(5,\frac{1}{2})$	$(3,\frac{3}{2})$	$(5,\frac{3}{2})$	$(5,\frac{1}{2})$	$(5,\frac{1}{2})$
H_{39} $(3,\frac{9}{2}^+)$	$(5,\frac{1}{2})$	$(5,\frac{1}{2})$	$(3,\frac{3}{2})$	$(5,\frac{3}{2})$	–	$(5,\frac{1}{2})$	$(3,\frac{3}{2})$	$(5,\frac{3}{2})$	–	$(5,\frac{1}{2})$

TABLE II: Number of the data points of $\pi N \to \pi N$ amplitudes included in our fits. The data are from SAID analysis of 14196 data points of $\pi^+ p \to \pi^+ p$, 13895 of $\pi^- p \to \pi^- p$, and 2877 of $\pi^- p \to \pi^0 p$.

Partial Wave		Partial Wave		
S_{11}	65×2	S_{31}	65×2	
P_{11}	65×2	P_{31}	61×2	
P_{13}	61×2	P_{33}	65×2	
D_{13}	61×2	D_{33}	55×2	
D_{15}	61×2	D_{35}	45×2	
F_{15}	48×2	F_{35}	43×2	
F_{17}	32×2	F_{37}	44×2	
G_{17}	42×2	G_{37}	32×2	
G_{19}	28×2	G_{39}	32×2	
H_{19}	34×2	H_{39}	31×2	
Sum	994		946	1940

TABLE III: Number of data points of hadronic processes included in our fits. Data are from the compilation of Bonn-Gatchina.

	$d\sigma/d\Omega$	P	R	a	sum
$\pi^- p \to \eta p$	294	–	–	–	294
$\pi^- p \to K^0 \Lambda$	587	354	–	–	941
$\pi^- p \to K^0 \Sigma^0$	259	90	–	–	349
$\pi^+ p \to K^+ \Sigma^+$	609	304	–	–	913
Sum	1749	748	–	–	2497

TABLE IV: The number of data points of photoproduction processes included in our fits. The data are from compilation of Bonn-Gatchina.

	$d\sigma/d\Omega$	Σ	T	P	G	H	E	F	$O_{x'}$	$O_{z'}$	$C_{x'}$	$C_{z'}$	sum
$\gamma p \to \pi^0 p$	4414	1866	389	607	75	71	140	–	7	7	–	–	7576
$\gamma p \to \pi^+ n$	2475	899	661	252	86	128	231	–	–	–	–	–	4732
$\gamma p \to \eta p$	780	151	50	–	–	–	–	–	–	–	–	–	981
$\gamma p \to K^+ \Lambda$	1320	118	66	1336	–	–	–	–	160	159	66	66	3291
$\gamma p \to K^+ \Sigma^0$	1280	87	–	95	–	–	–	–	–	–	94	94	1650
$\gamma p \to K^0 \Sigma^+$	276	15	–	72	–	–	–	–	–	–	–	–	363
Sum	10545	3136	1166	2362	161	199	371	–	167	166	160	160	18593

TABLE V: Observables and number of the data points considered in this coupled-channels analysis. The data are taken from the database of the INS DAC Services.

Reactions	Observables	Number of data points
γ'n' $\to \pi^- p$	$d\sigma/d\Omega$	2305
	Σ	308
	T	94
	P	88
γ'n' $\to \pi^0 n$	$d\sigma/d\Omega$	148
	Σ	216
Sum		3159

TABLE VI: Number of data points of $p(e, e'\pi)N$ included in our fits. The data are for about 25 Q^2 with $W < 2000$ MeV.

	$\sigma_T + \epsilon\sigma_L$	σ_{TT}	σ_{LT}	σ'_{LT}	sum
$p(e, e'\pi^0)p$	5830	5830	5830	240	17730
$p(e, e'\pi^+)n$	2614	2614	2614	566	8408
Sum	8444	8444	8444	806	26138

VI. RESULTS

The nucleon resonance properties extracted from ANL-Osaka amplitudes were finalized in 2016 and published in Ref. [17]. In Table VII, we list the pole positions and the residues $R_{\pi N,\pi N}$ of the extracted resonances. In Ref. [16], the residues for $R_{\pi N,\eta N}$, $R_{\pi N,K\Lambda}$, and $R_{\pi N,K\Sigma}$ are also given. However these results are not as solid as that of $R_{\pi N,\pi N}$ because the data of $\pi N \to \eta N, K\Lambda, K\Sigma$ included in the fits are not as accurate as the data of $\pi N \to \pi N$. The residues associated with the unstable channels $\pi\Delta, \rho N$ and σN are also not given because the analytic continuation of the PWA associated with these channels to complex E-plane is rather complex and a rigorous way to do this remains to be explored.

The determined helicity amplitudes for the $\gamma p \to N^*$ transition at resonance pole positions, published in Ref. [17], are listed in Table VIII. However the Q^2-dependence of $\gamma p \to N^*$ transitions at resonance pole was not extracted because only the data at few Q^2 were included in the fits.

To illustrate the quality of our fits to the data, we present sample results from our analysis in the Appendix: (A) Total cross sections of πN reactions, (B) Total cross sections of γN reactions, (C) Differential cross sections of $\pi N \to \pi N, \eta N,\ K\Lambda, K\Sigma$, (D) Differential cross sections of $\gamma N \to \pi N, \eta N,\ K\Lambda, K\Sigma$, (E) Differential cross sections of $\gamma^* N \to \pi N$, (F) Inclusive cross sections of $p(e, e')$.

TABLE VII: The extracted nucleon resonance pole mass (M_R) and πN elastic residue ($R_{\pi N,\pi N}$). M_R is listed as $(\mathrm{Re}(M_R), -\mathrm{Im}(M_R))$ in units of MeV, while $R_{\pi N,\pi N} = |R_{\pi N,\pi N}|e^{i\phi}$ is listed as $(|R_{\pi N,\pi N}|, \phi)$ in units of MeV for $|R_{\pi N,\pi N}|$ and degree for ϕ. The range of ϕ is taken to be $-180^\circ \leq \phi < 180^\circ$. The N^* resonances for which the asterisk (*) is marked locate in the complex energy plane slightly off the sheet closest to the physical real energy axis, yet are still expected to visibly affect the physical observables.

	$J^P(L_{2I2J})$	M_R	$R_{\pi N,\pi N}$
N^*	$1/2^-(S_{11})$	(1490, 102)	(70, −42)
		(1652, 71)	(45, −74)
	$1/2^+(P_{11})$	(1376, 75)	(38, −70)
		(1741, 139)	(15, 80)
	$3/2^+(P_{13})$	(1708, 65)	(9, −4)
		(1765, 160)	(30, −105)
	$3/2^-(D_{13})$	(1509, 48)	(30, −10)
		(1702, 148)*	(< 1, −161)
	$5/2^-(D_{15})$	(1651, 68)	(26, −27)
	$5/2^+(F_{15})$	(1665, 52)	(36, −22)
Δ^*	$1/2^-(S_{31})$	(1597, 69)	(21, −111)
		(1713, 187)	(20, 73)
	$1/2^+(P_{31})$	(1857, 145)	(11, −118)
	$3/2^+(P_{33})$	(1212, 52)	(55, −47)
		(1733, 162)	(16, −108)
	$3/2^-(D_{33})$	(1577, 113)	(13, −67)
	$5/2^-(D_{35})$	(1911, 130)	(4, −30)
	$5/2^+(F_{35})$	(1767, 88)	(11, −61)
	$7/2^+(F_{37})$	(1885, 102)	(49, −30)

TABLE VIII: The determined helicity amplitudes for the $\gamma p \to N^*$ transition at resonance pole positions. The presented values follow the notation: $A_{1/2,3/2} = \bar{A}_{1/2,3/2} \times e^{i\phi}$ with ϕ taken to be in the range $-90^\circ \leq \phi < 90^\circ$. The units of $\bar{A}_{1/2,3/2}$ and ϕ are 10^{-3} GeV$^{-1/2}$ and degree, respectively. Each resonance is specified by the isospin and spin-parity quantum numbers as well as the real part of the resonance pole mass.

Particle $J^P(L_{2I2J})$	$\bar{A}_{1/2}$	ϕ	$\bar{A}_{3/2}$	ϕ
$N(1490)1/2^-(S_{11})$	160	8	-	-
$N(1652)1/2^-(S_{11})$	36	-28	-	-
$N(1376)1/2^+(P_{11})$	-40	-8	-	-
$N(1741)1/2^+(P_{11})$	-47	-24	-	-
$N(1708)3/2^+(P_{13})$	131	7	-33	12
$N(1765)3/2^+(P_{13})$	123	-11	-71	3
$N(1509)3/2^-(D_{13})$	-28	< 1	102	4
$N(1703)3/2^-(D_{13})$	13	50	31	-71
$N(1651)5/2^-(D_{15})$	8	19	49	-12
$N(1665)5/2^+(F_{15})$	-44	-11	60	-2
$\Delta(1597)1/2^-(S_{31})$	105	1	-	-
$\Delta(1713)1/2^-(S_{31})$	40	13	-	-
$\Delta(1857)1/2^+(P_{31})$	-1	-78	-	-
$\Delta(1212)3/2^+(P_{33})$	-134	-16	-257	-3
$\Delta(1733)3/2^+(P_{33})$	-48	63	-94	74
$\Delta(1577)3/2^-(D_{33})$	128	19	119	46
$\Delta(1911)5/2^-(D_{35})$	48	-22	11	-36
$\Delta(1767)5/2^+(F_{35})$	38	-7	-24	-80
$\Delta(1885)7/2^+(F_{37})$	-69	-14	-83	2

TABLE IX: The isovector and isoscalar helicity amplitudes for $\gamma N \to N^*$ are defined as $A_\lambda^{T=1} = (A_\lambda^p - A_\lambda^n)$, and $A_\lambda^{T=0} = (A_\lambda^p + A_\lambda^n)$, where A_λ^p and A_λ^n are the helicity amplitudes of $\gamma p \to N^*$ and $\gamma n \to N^*$, respectively. See the caption of Table VIII for the notation of the table.

Particle $J^P(L_{2I2J})$	$\bar{A}_{1/2}^{T=1}$	ϕ	$\bar{A}_{1/2}^{T=0}$	ϕ	$\bar{A}_{3/2}^{T=1}$	ϕ	$\bar{A}_{3/2}^{T=0}$	ϕ
$N(1490)1/2^-(S_{11})$	136	11	26	−10	-	-	-	-
$N(1652)1/2^-(S_{11})$	19	−29	18	−28	-	-	-	-
$N(1376)1/2^+(P_{11})$	−68	−13	28	−21	-	-	-	-
$N(1741)1/2^+(P_{11})$	−120	−11	75	−3	-	-	-	-
$N(1708)3/2^+(P_{13})$	95	7	36	8	−9	68	−29	−2
$N(1765)3/2^+(P_{13})$	78	−10	45	−14	−55	4	−16	−2
$N(1509)3/2^-(D_{13})$	7	−2	−35	−1	106	4	−5	8
$N(1703)3/2^-(D_{13})$	20	−28	−22	−63	54	−61	−24	−48
$N(1651)5/2^-(D_{15})$	42	4	−34	1	44	−8	6	−37
$N(1665)5/2^+(F_{15})$	−39	−11	−5	−8	58	−3	2	18

Acknowledgments

This work is supported by the U.S. Department of Energy, Office of Science, Office of Nuclear Physics, Contract No. DE-AC02-06CH11357.

Appendix A: Total Cross sections of πN reactions

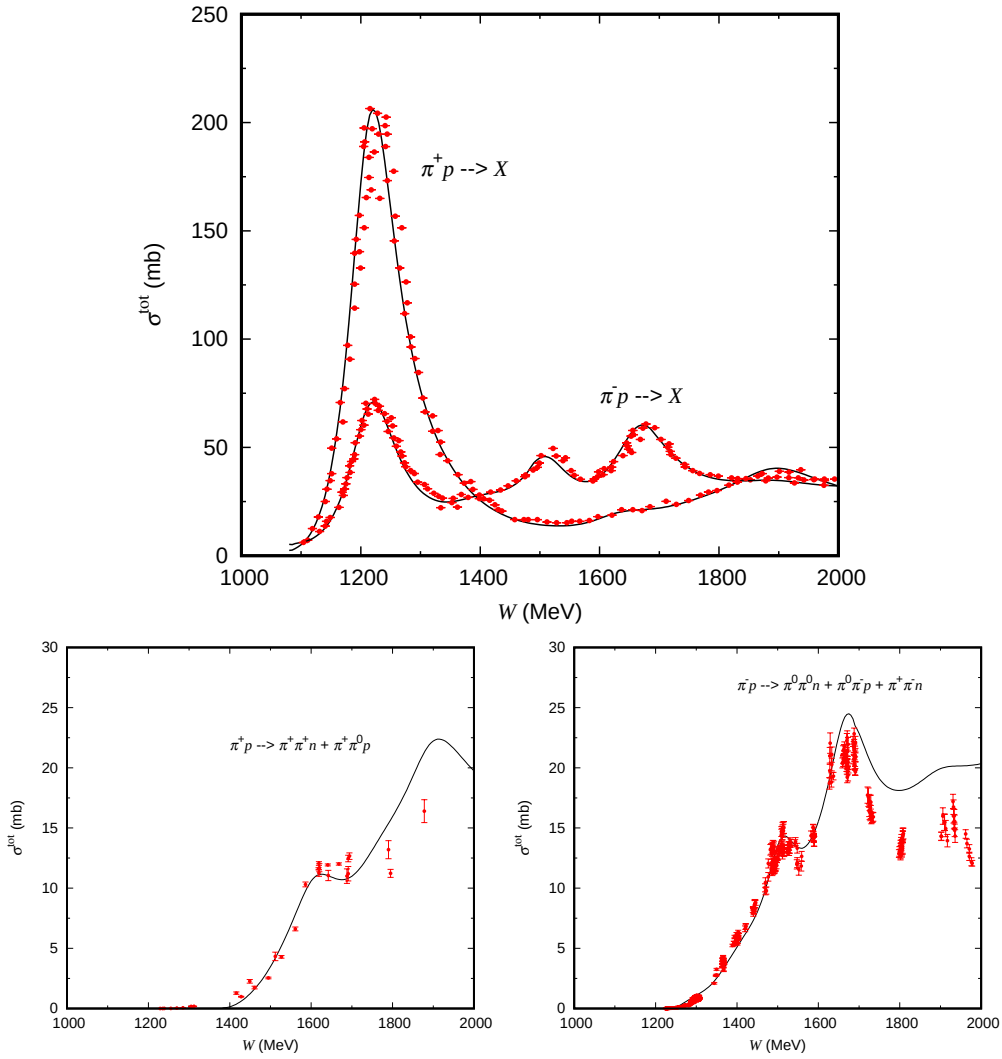

FIG. 6: σ^{tot} of $\pi^{\pm}p \to X, \pi\pi N$

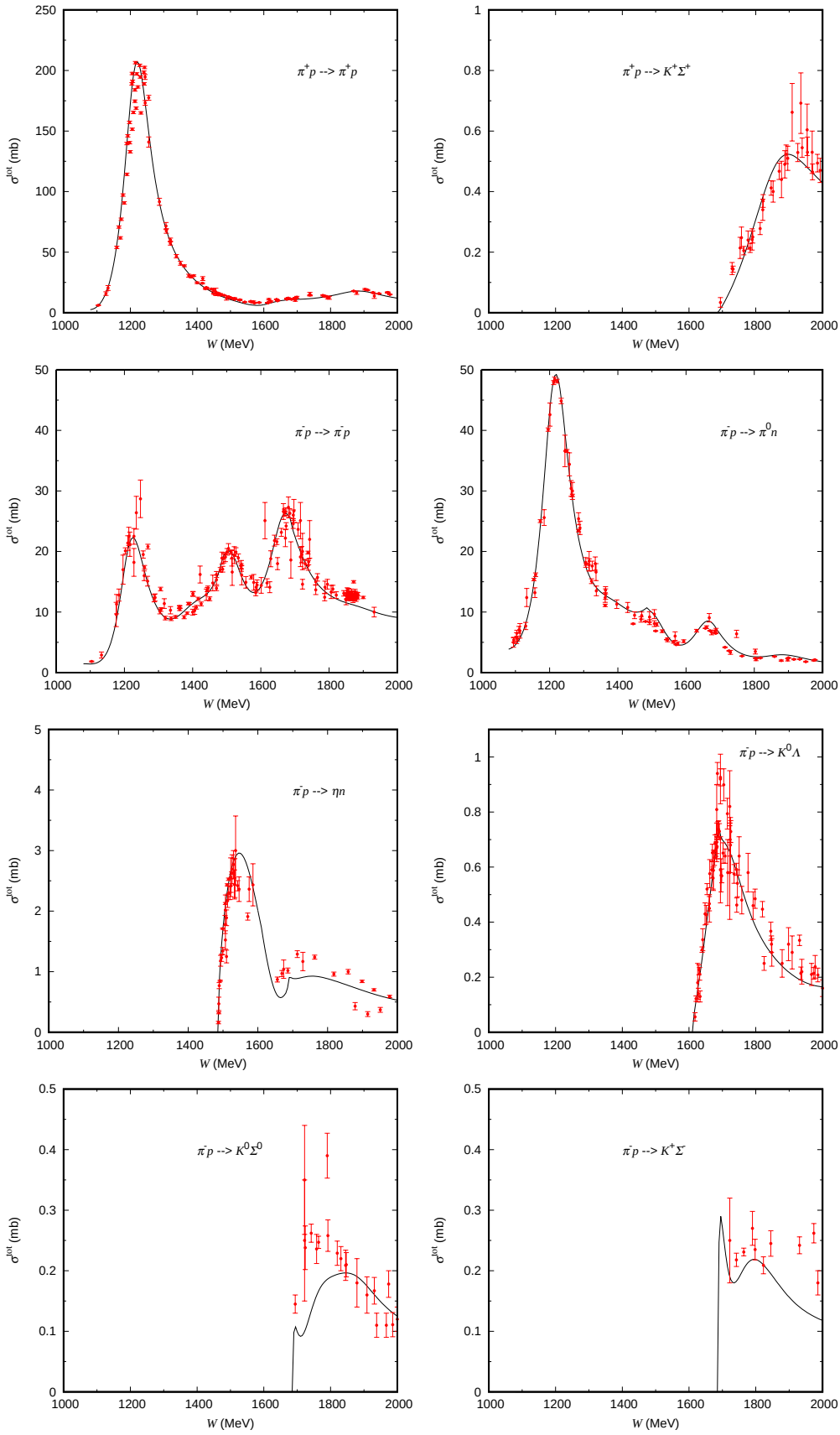

FIG. 7: σ^{tot} of $\pi^{\pm}p \to \pi N, \eta N, K\Lambda, K\Sigma$

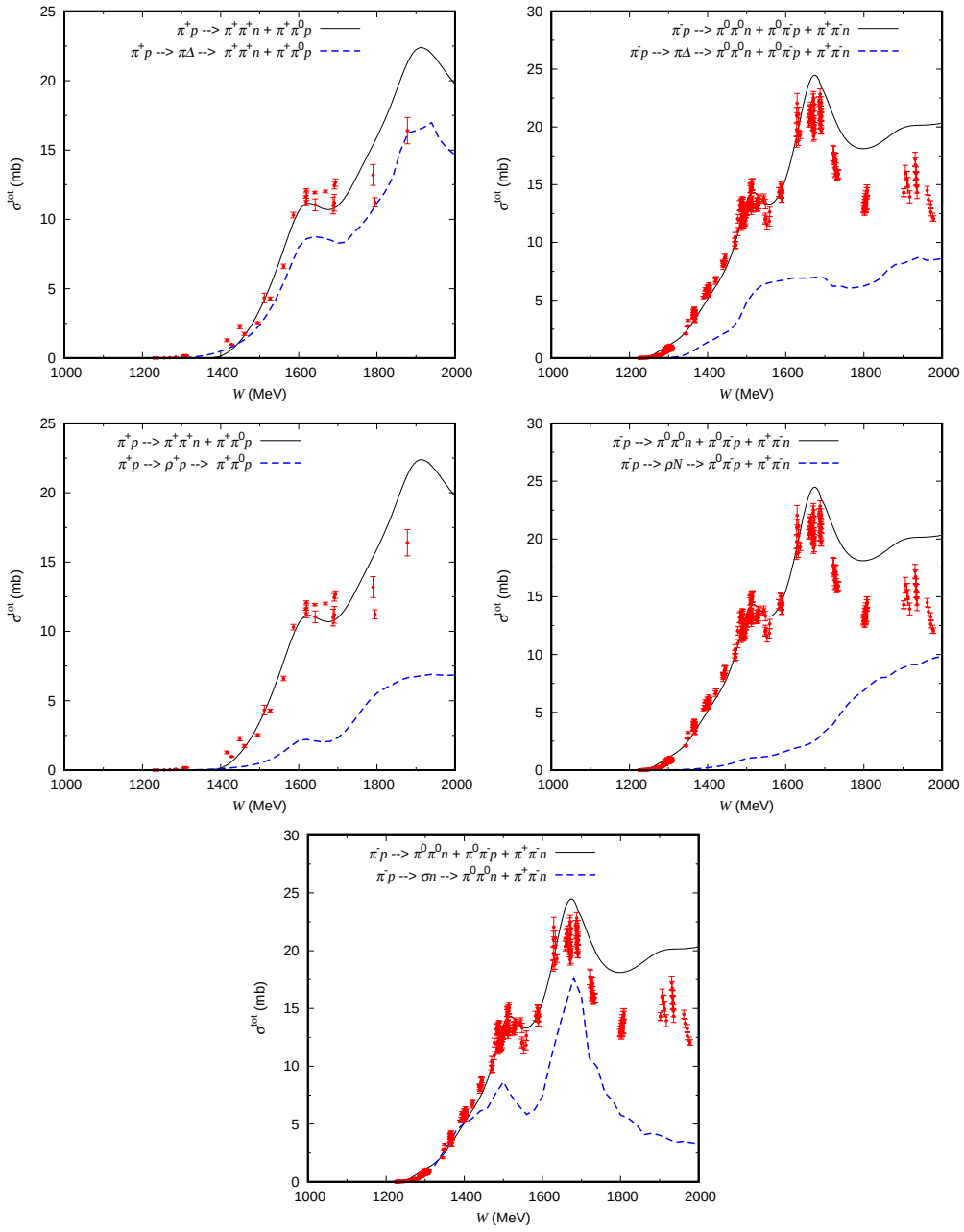

FIG. 8: Total cross sections for $\pi^{\pm}p \to (MB)^R \to \pi\pi N$ (dashed curves) are compared with $\pi^{\pm}p \to \pi\pi N$(solid curves). Top row: $(MB)^R = \pi\Delta$; middle row: $(MB)^R = \rho N$; bottom row:$(MB)^R = \sigma N$.

Appendix B: Total Cross sections of γN reactions

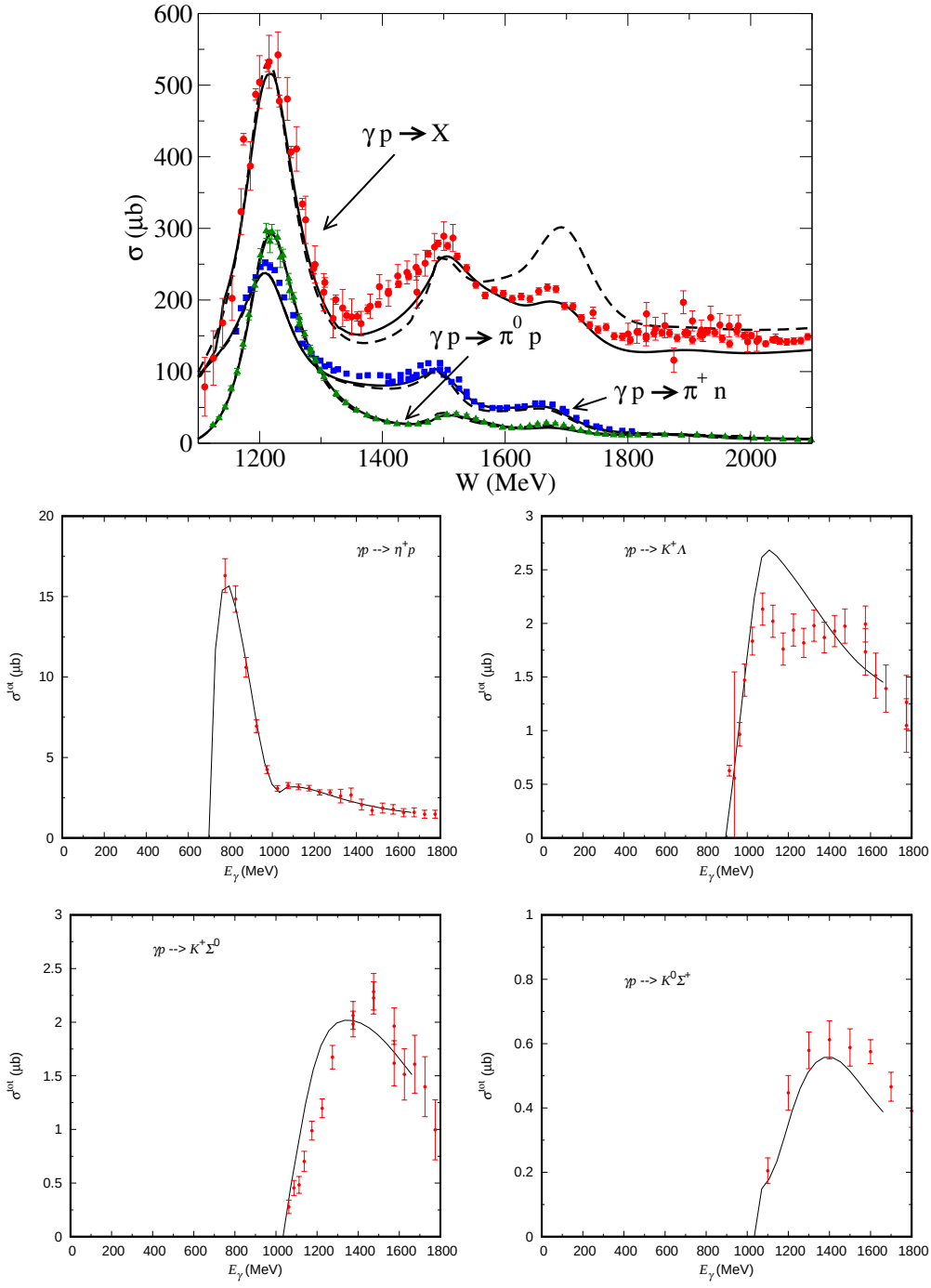

FIG. 9: Top :$\gamma p \to X, \pi^0 p, \pi^+ n$, dashed curves are our previous analysis; Lower four figures: $\gamma p \to \eta p, K\Lambda, K^+\Sigma^0, K^0\Sigma^+$.

Appendix C: Differential cross sections of πN reactions

1. $\pi N \to \pi N$

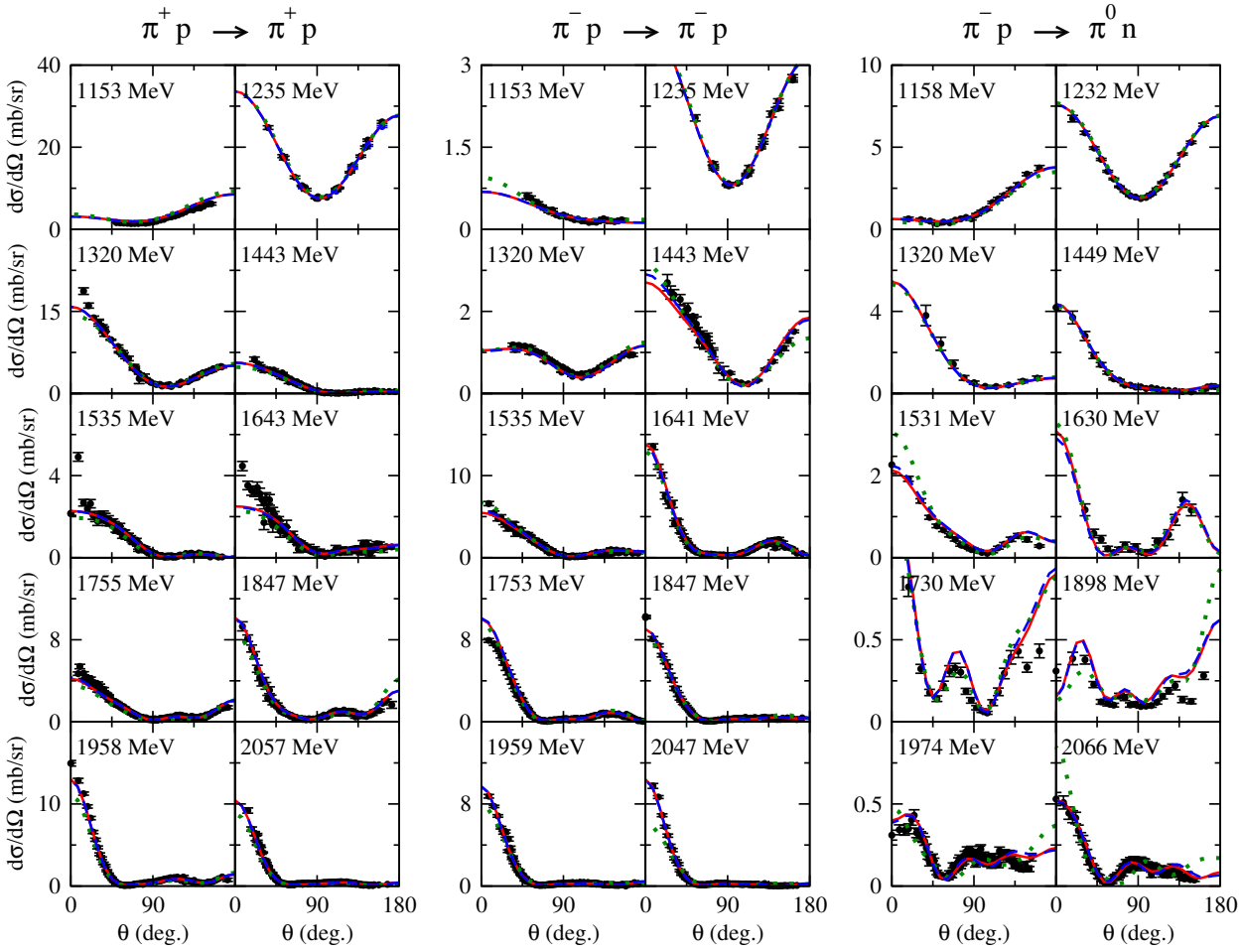

FIG. 10: Differential cross section for $\pi N \to \pi N$. The red solid curves are the current results while the blue dashed curves are from our previous analysis of 2007.

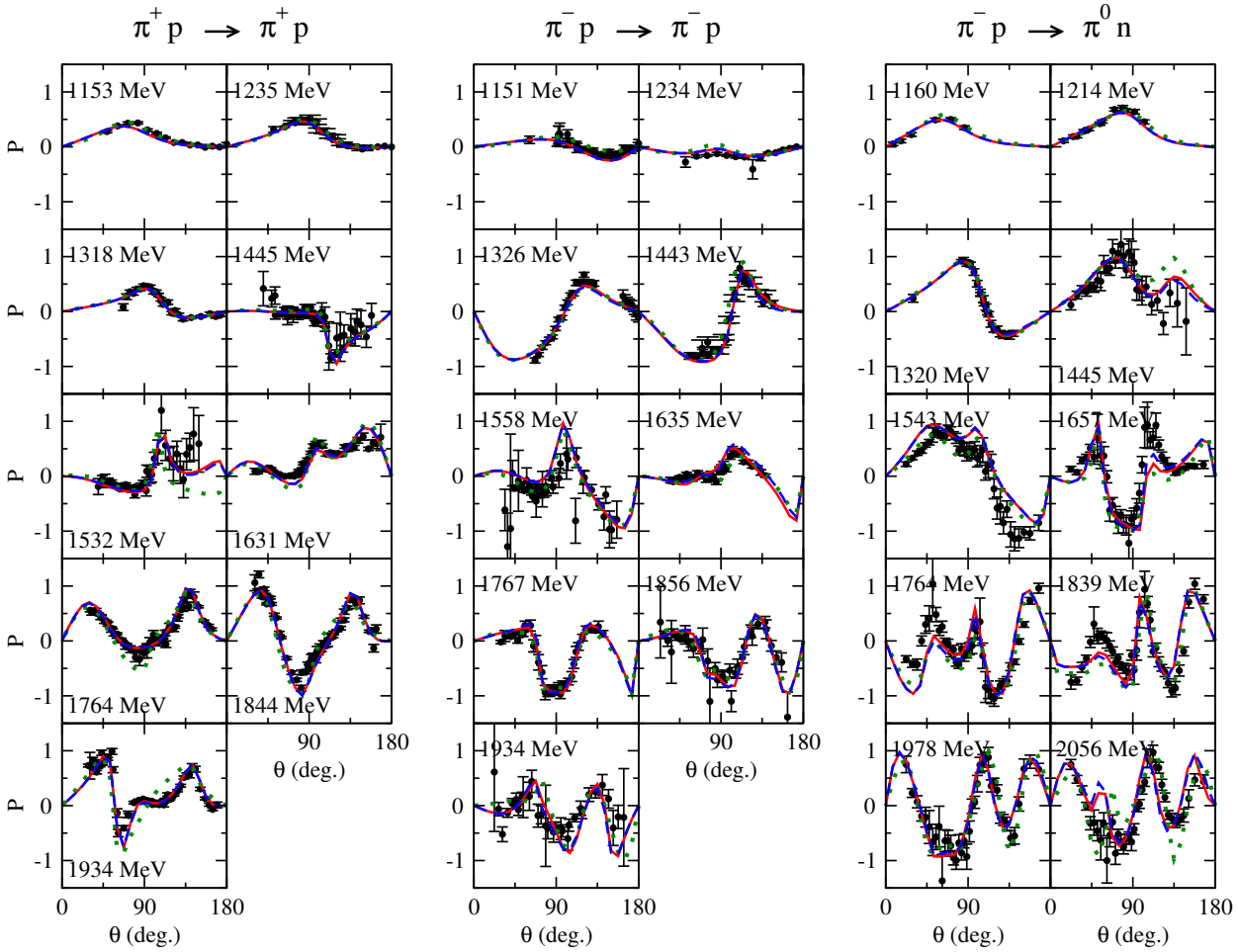

FIG. 11: The target polarization P of $\pi N \to \pi N$. The red solid curves are the current results while the blue dashed curves are from our previous analysis of 2007.

2. $\pi N \to \eta N$

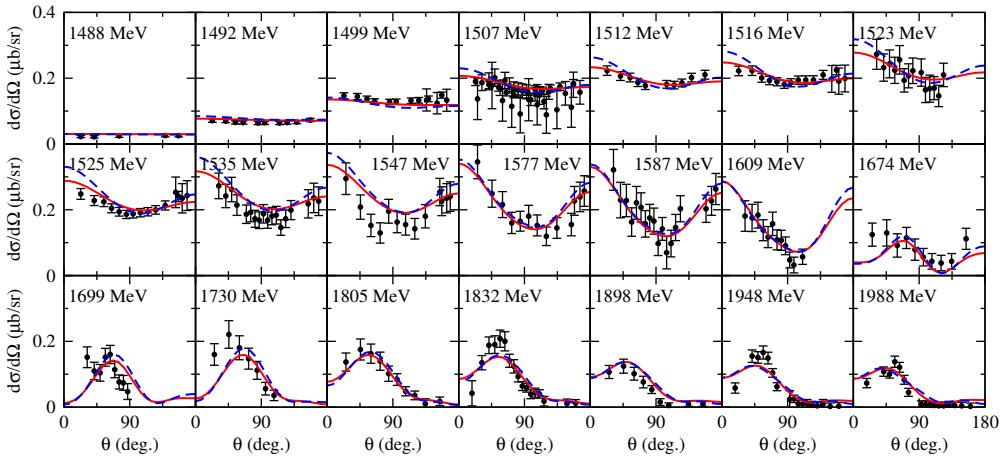

FIG. 12: Differential cross sections of $\pi^- p \to \eta n$. The red solid curves are the current results while the blue dashed curves are from our previous analysis of 2007.

3. $\pi N \to K\Lambda$

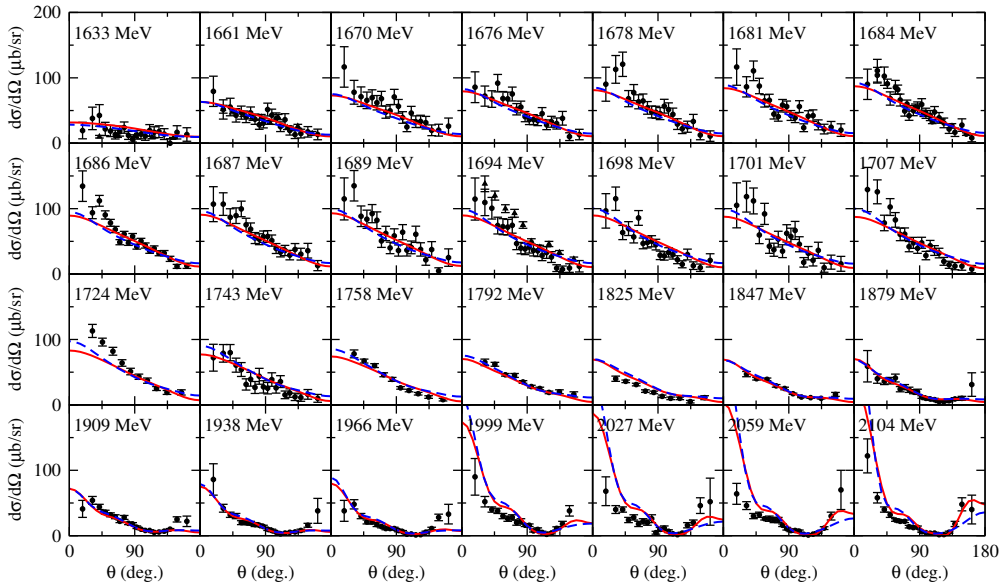

FIG. 13: Differential cross sections of $\pi^- p \to K^0 \Lambda^0$. The red solid curves are the current results while the blue dashed curves are from our previous analysis of 2007.

4. $\pi N \to K\Sigma$

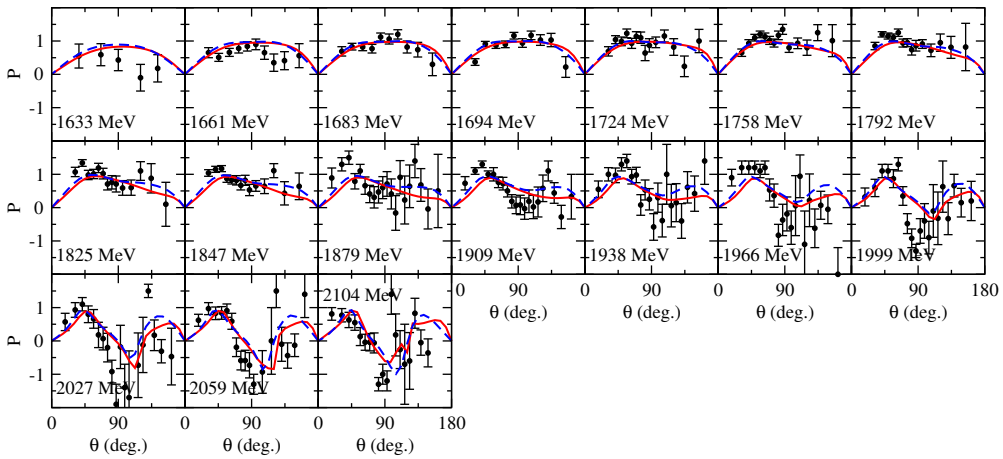

FIG. 14: Differential cross sections of $\pi^- p \to K^0\Lambda^0$. The red solid curves are the current results while the blue dashed curves are from our previous analysis of 2007.

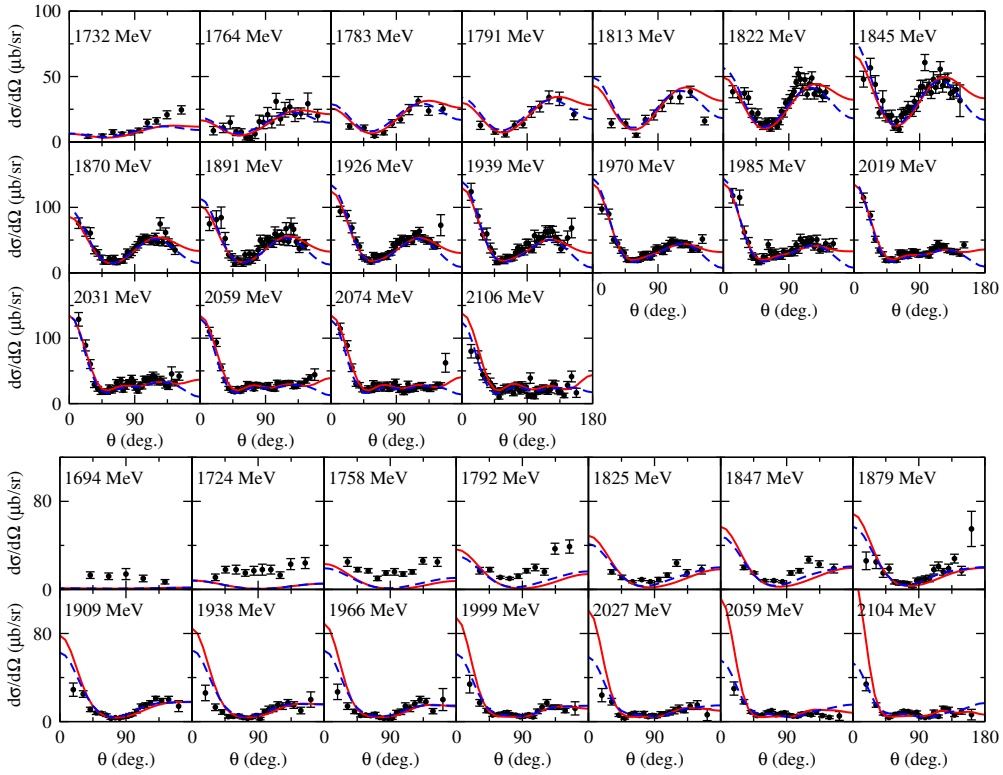

FIG. 15: Differential cross sections of $\pi^+ p \to K^+\Sigma^+$(upper) and $\pi^- p \to K^0\Sigma^0$(lower). The red solid curves are the current results while the blue dashed curves are from our previous analysis of 2007.

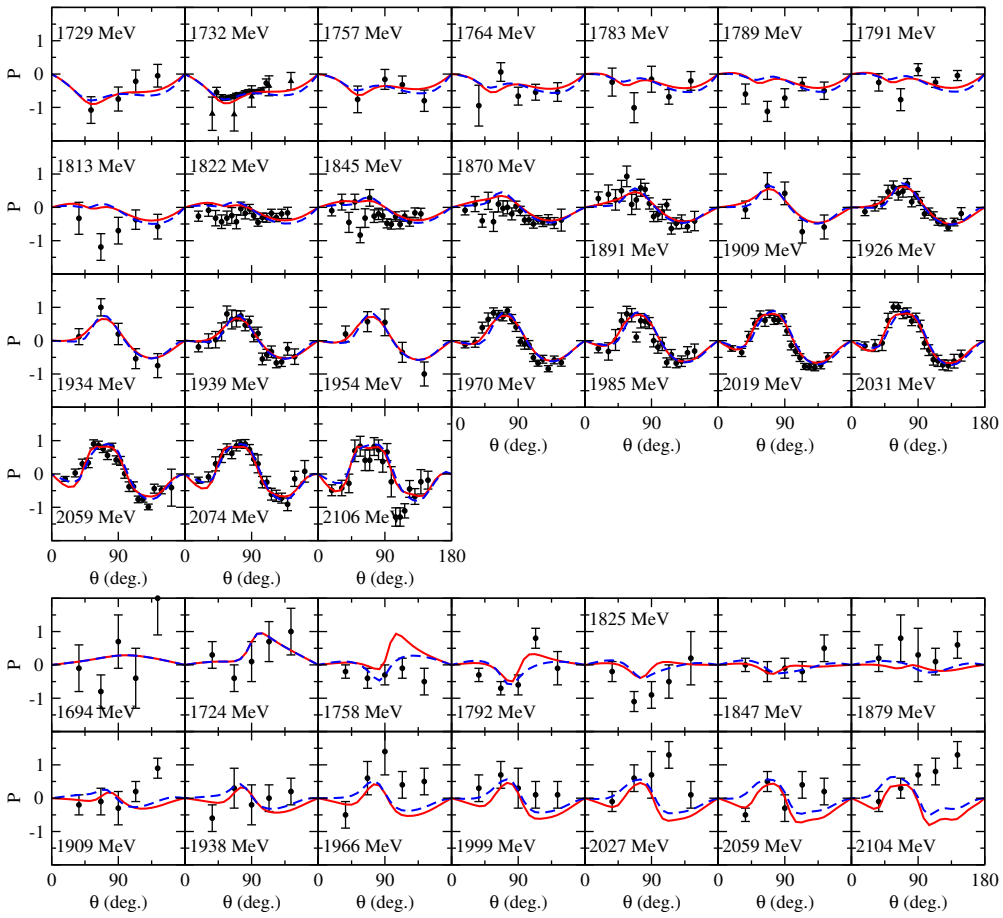

FIG. 16: Polarization P of $\pi^+ p \to K^+\Sigma^+$(upper) and $\pi^- p \to K^0\Sigma^0$(lower). The red solid curves are the current results while the blue dashed curves are from our previous analysis of 2007.

Appendix D: Differential Cross sections of $\gamma N \to \pi N, \eta N, K\Lambda, K\Sigma$

1. $\gamma p \to \pi^0 p$

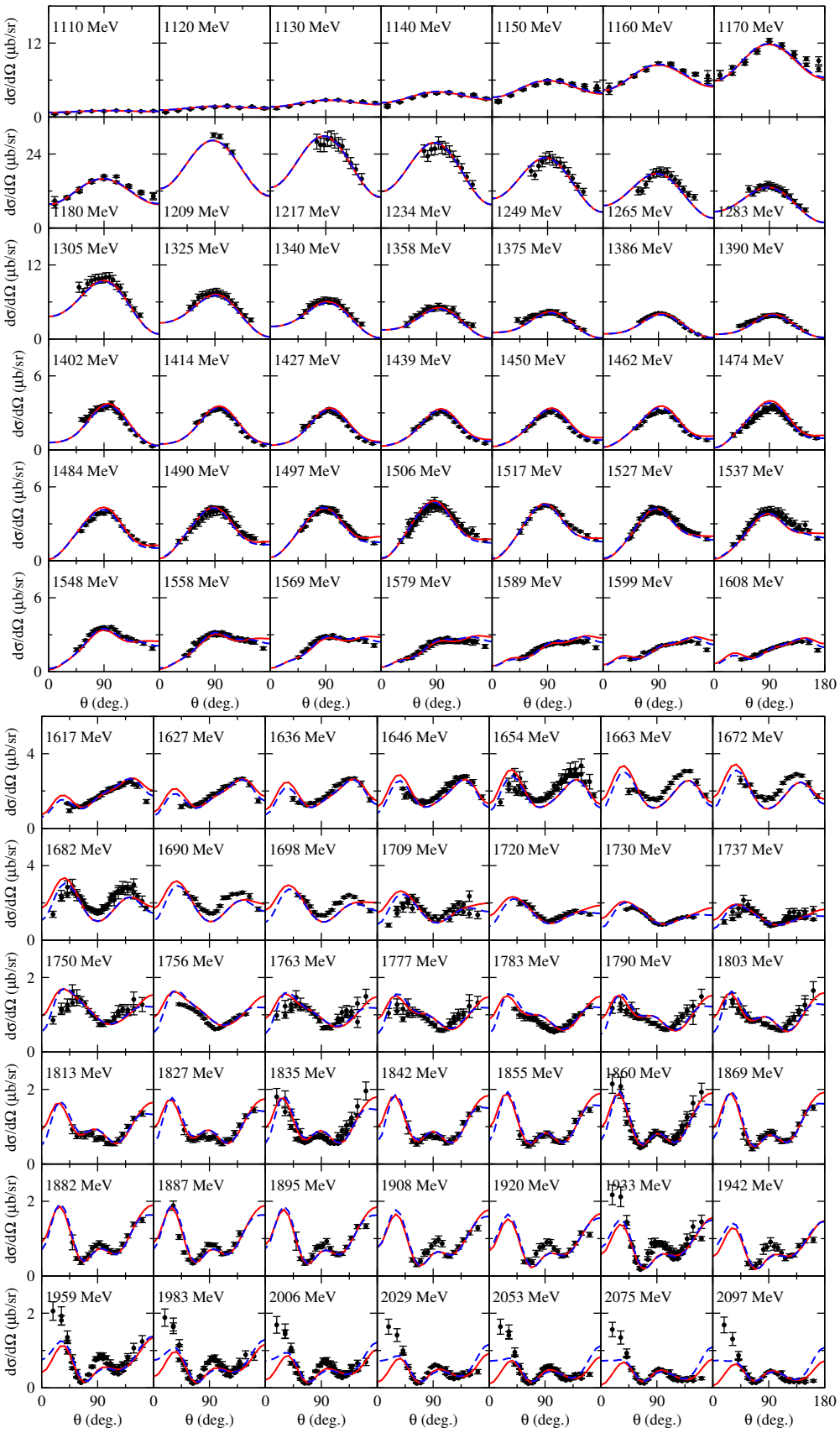

FIG. 17: Differential cross sections of $\gamma p \to \pi^0 p$. The red solid curves are the current results while the blue dashed curves are from our previous analysis.

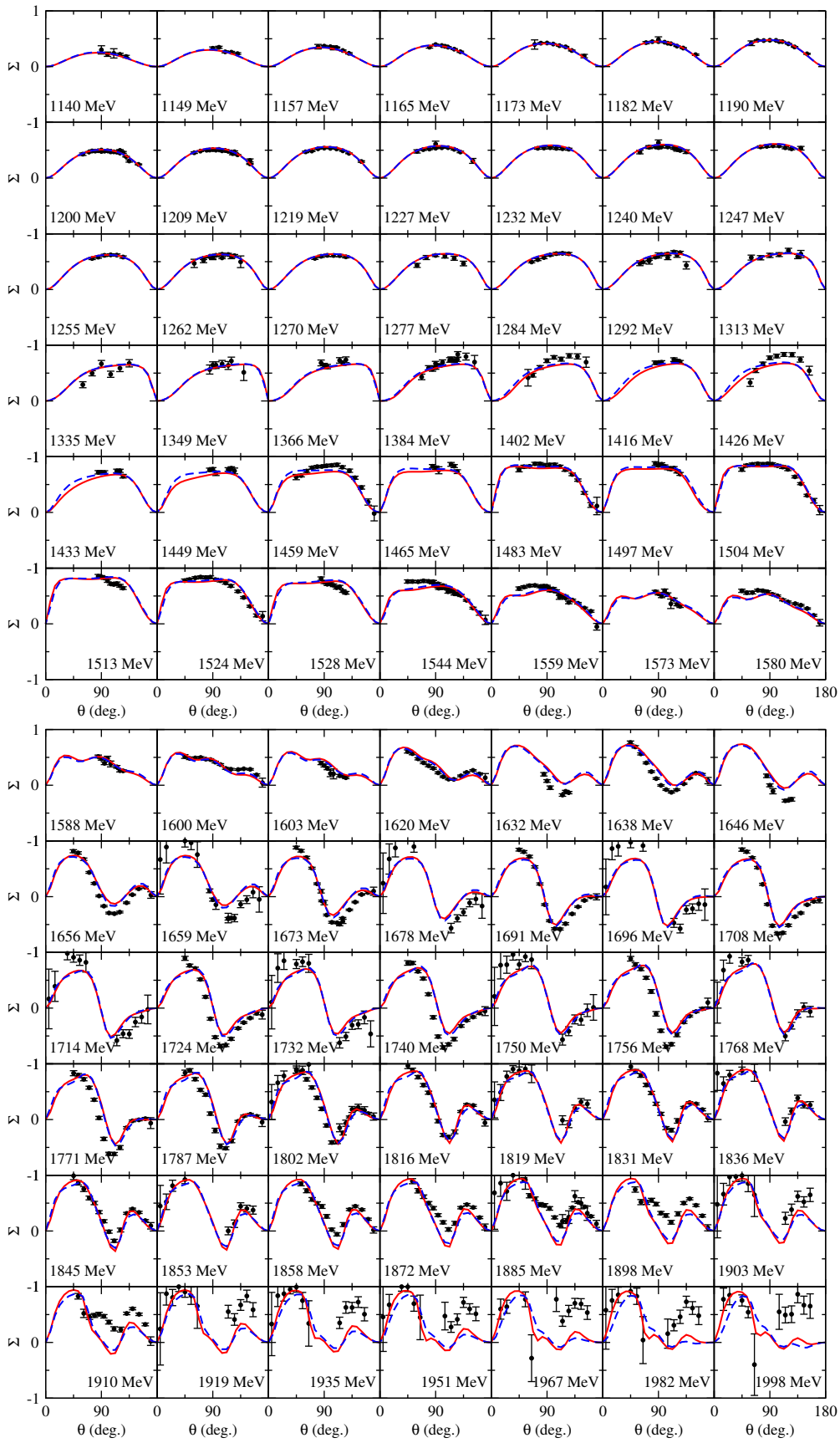

FIG. 18: The photon asymmetries Σ of $\gamma p \to \pi^0 p$. The red solid curves are the current results while the blue dashed curves are from our previous analysis.

2. $\gamma p \to \pi^+ n$

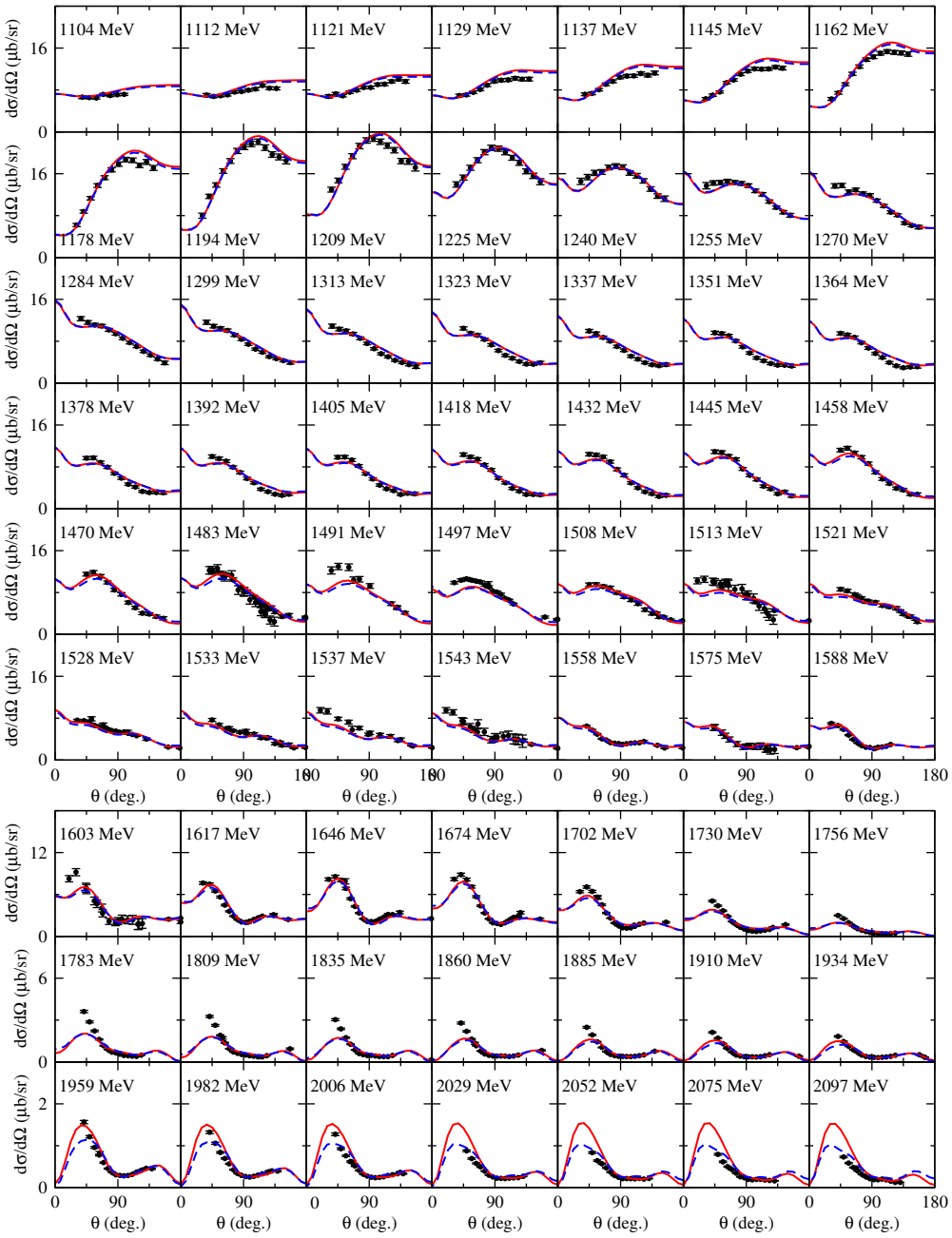

FIG. 19: Differential cross sections of $\gamma p \to \pi^+ n$. The red solid curves are the current results while the blue dashed curves are from our previous analysis.

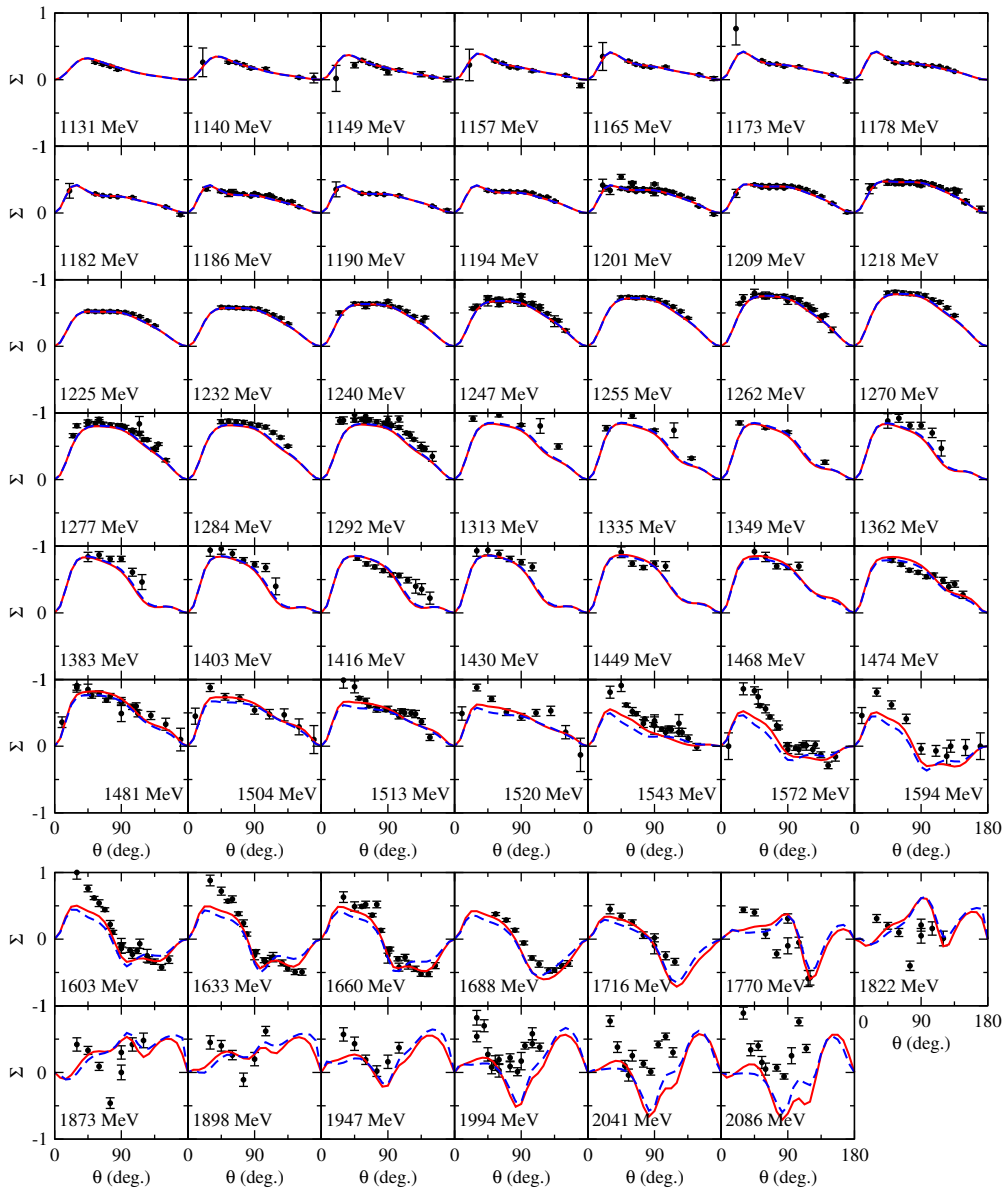

FIG. 20: The photon asymmetries Σ of $\gamma p \to \pi^+ n$. The red solid curves are the current results while the blue dashed curves are from our previous analysis.

3. $\gamma p \to \eta p$

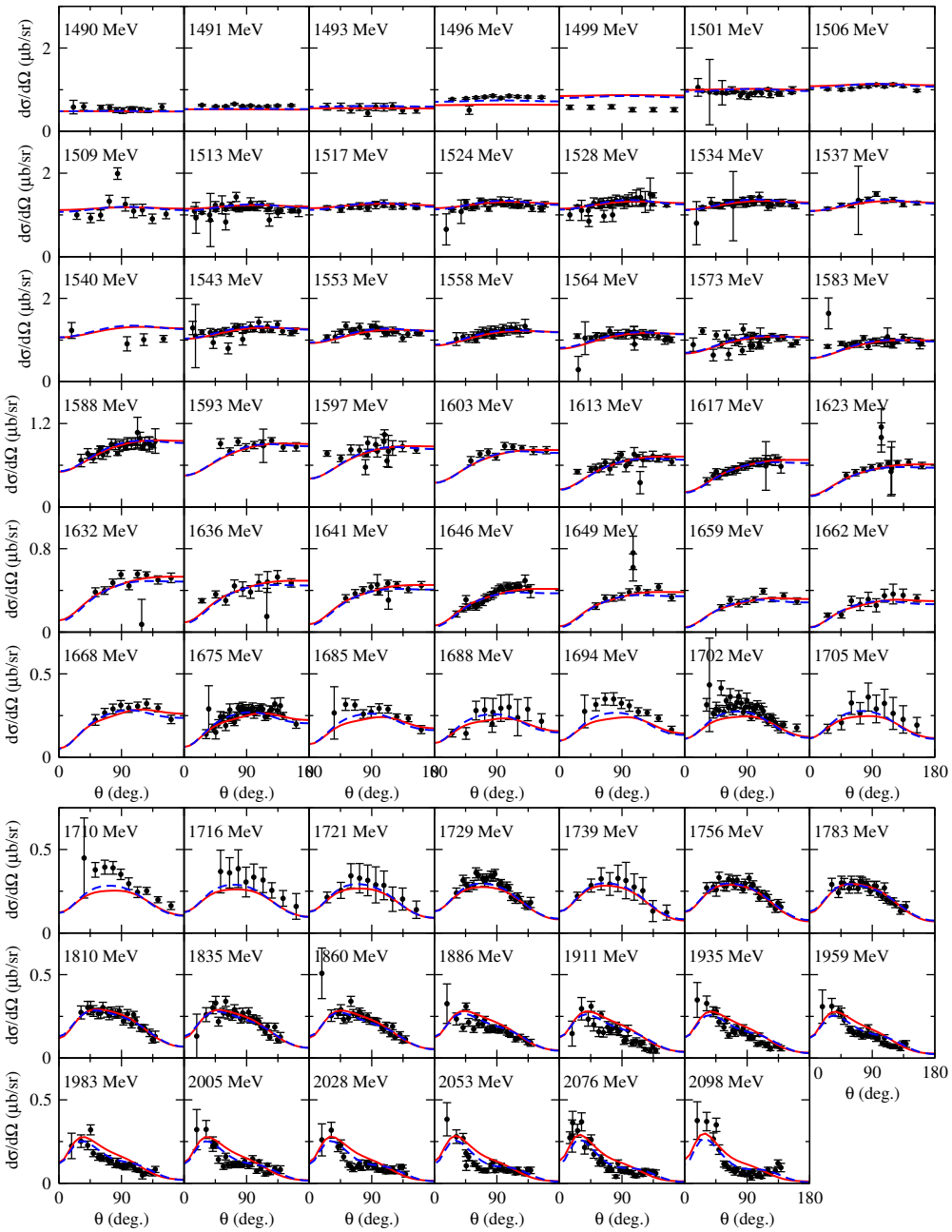

FIG. 21: Differential cross sections of $\gamma p \to \eta p$. The red solid curves are the current results while the blue dashed curves are from our previous analysis.

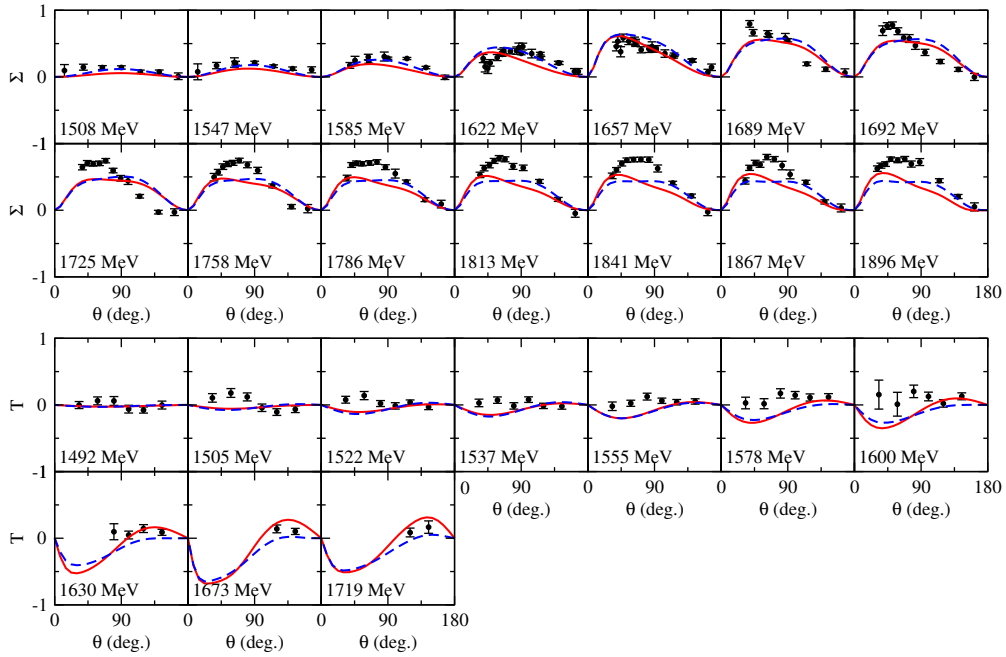

FIG. 22: Σ and T of $\gamma p \to \eta p$. The red solid curves are the current results while the blue dashed curves are from our previous analysis.

4. $\gamma p \to K^+\Lambda$

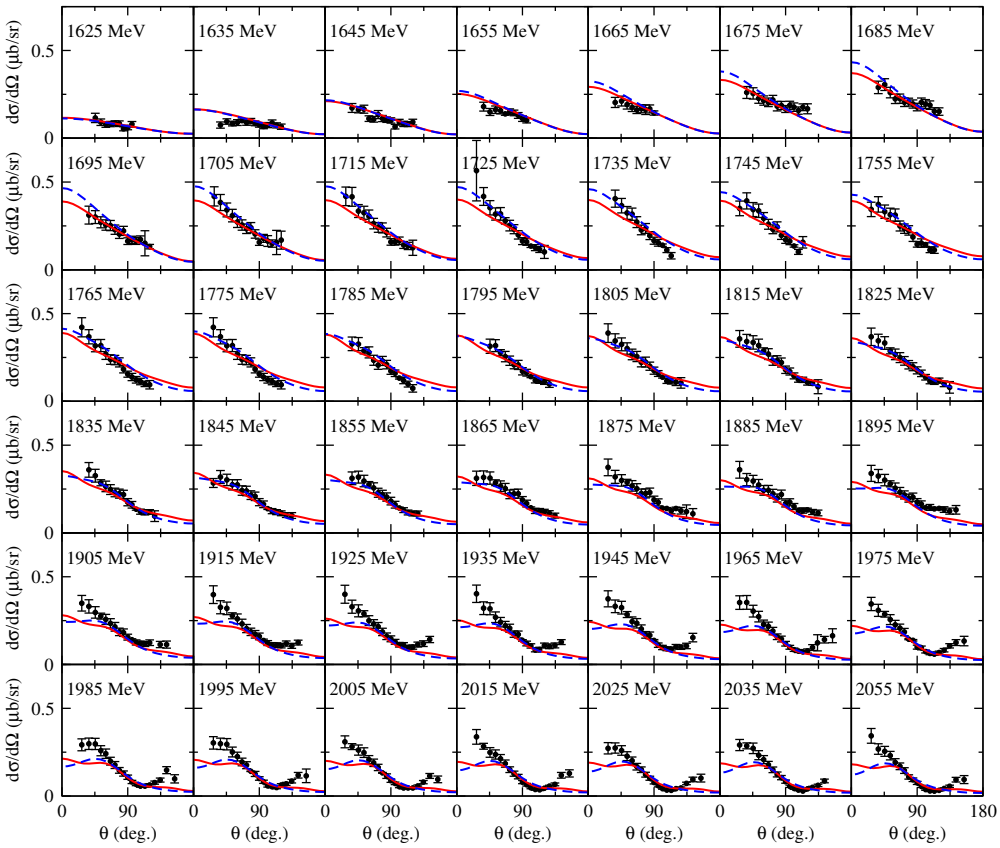

FIG. 23: Differential cross sections of $\gamma p \to K^+\Lambda$. The red solid curves are the current results while the blue dashed curves are from our previous analysis.

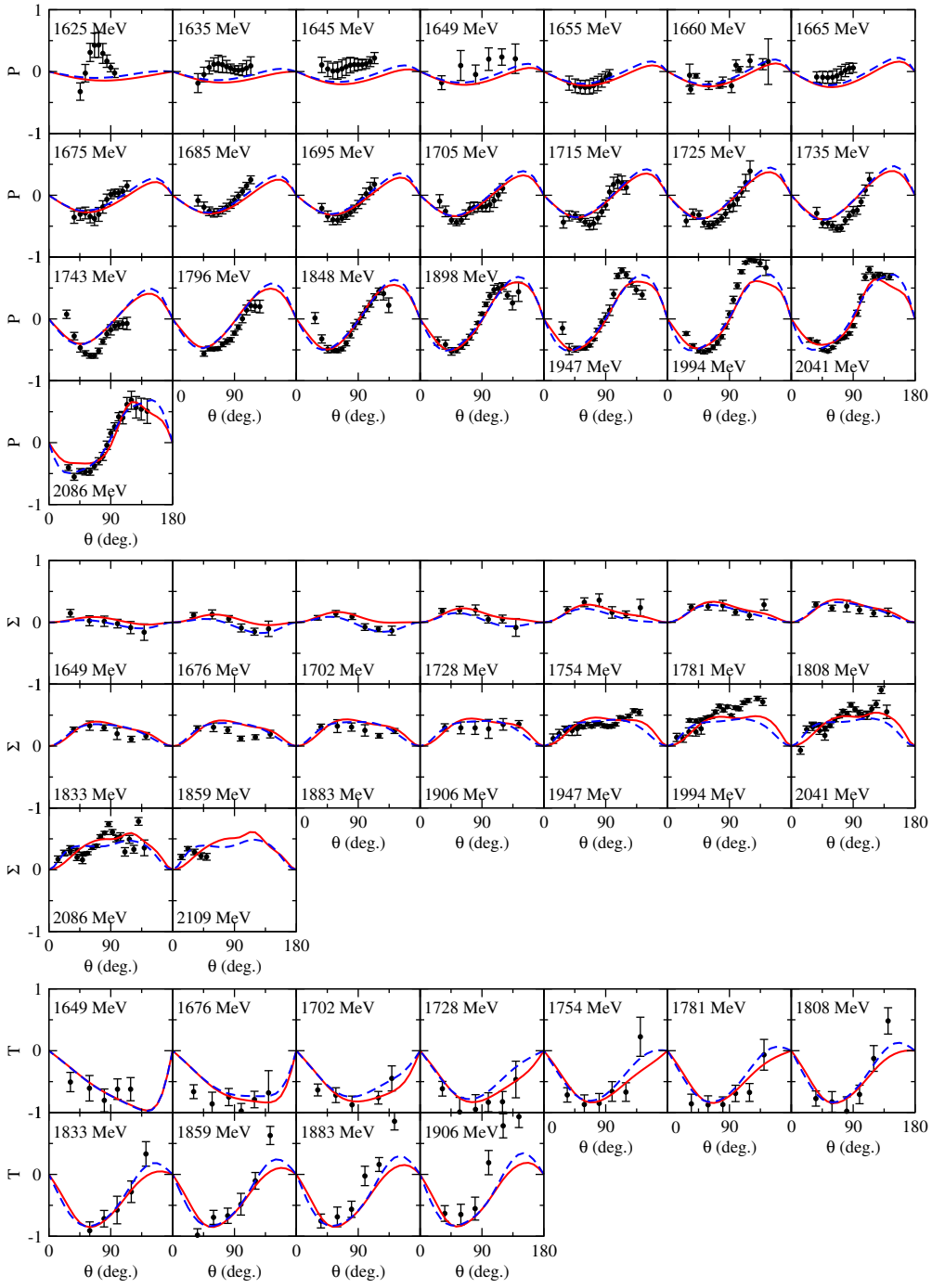

FIG. 24: Observables P, Σ, T of of $\gamma p \to K^+\Lambda$. The red solid curves are the current results while the blue dashed curves are from our previous analysis.

5. $\gamma p \to K\Sigma$

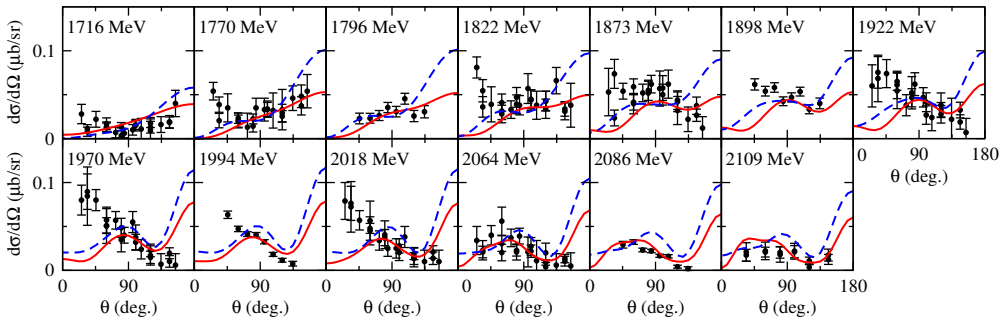

FIG. 25: Differential cross sections of $\gamma p \to K^0\Sigma^+$. The red solid curves are the current results while the blue dashed curves are from our previous analysis.

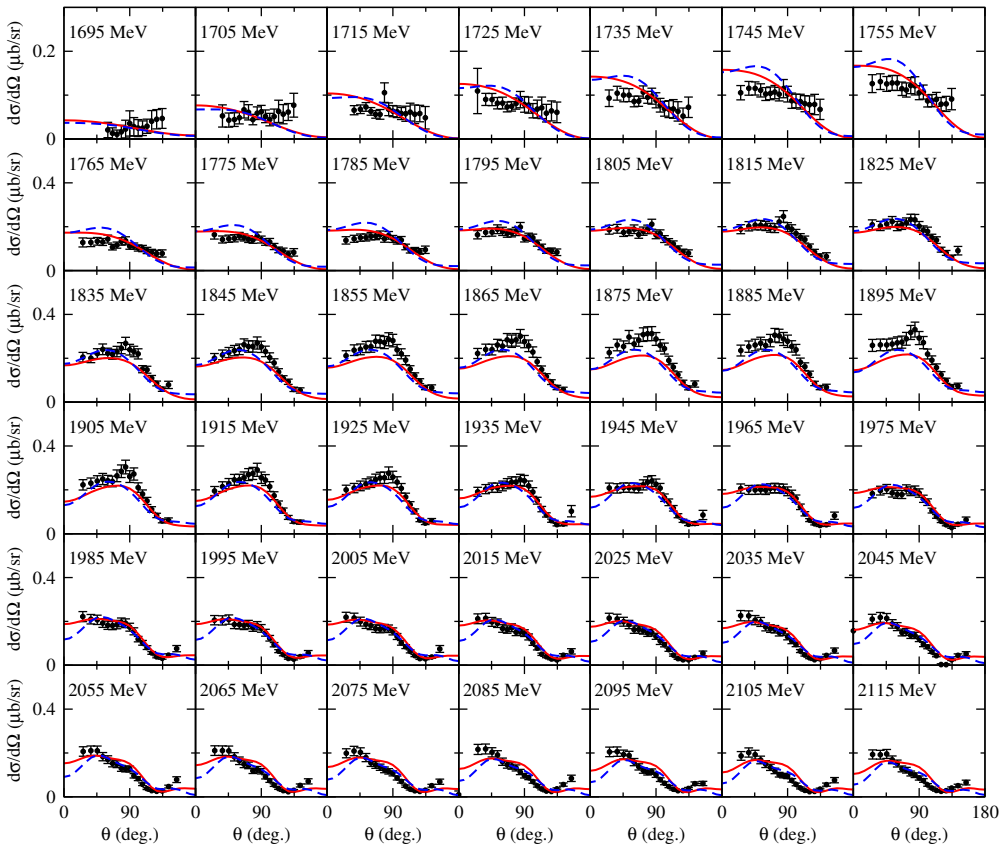

FIG. 26: Differential cross sections of $\gamma p \to K^+\Sigma^0$. The red solid curves are the current results while the blue dashed curves are from our previous analysis.

Appendix E: Differential Cross sections of $\gamma^* p \to \pi N$ reactions

1. $\gamma^* p \to \pi^0 p$

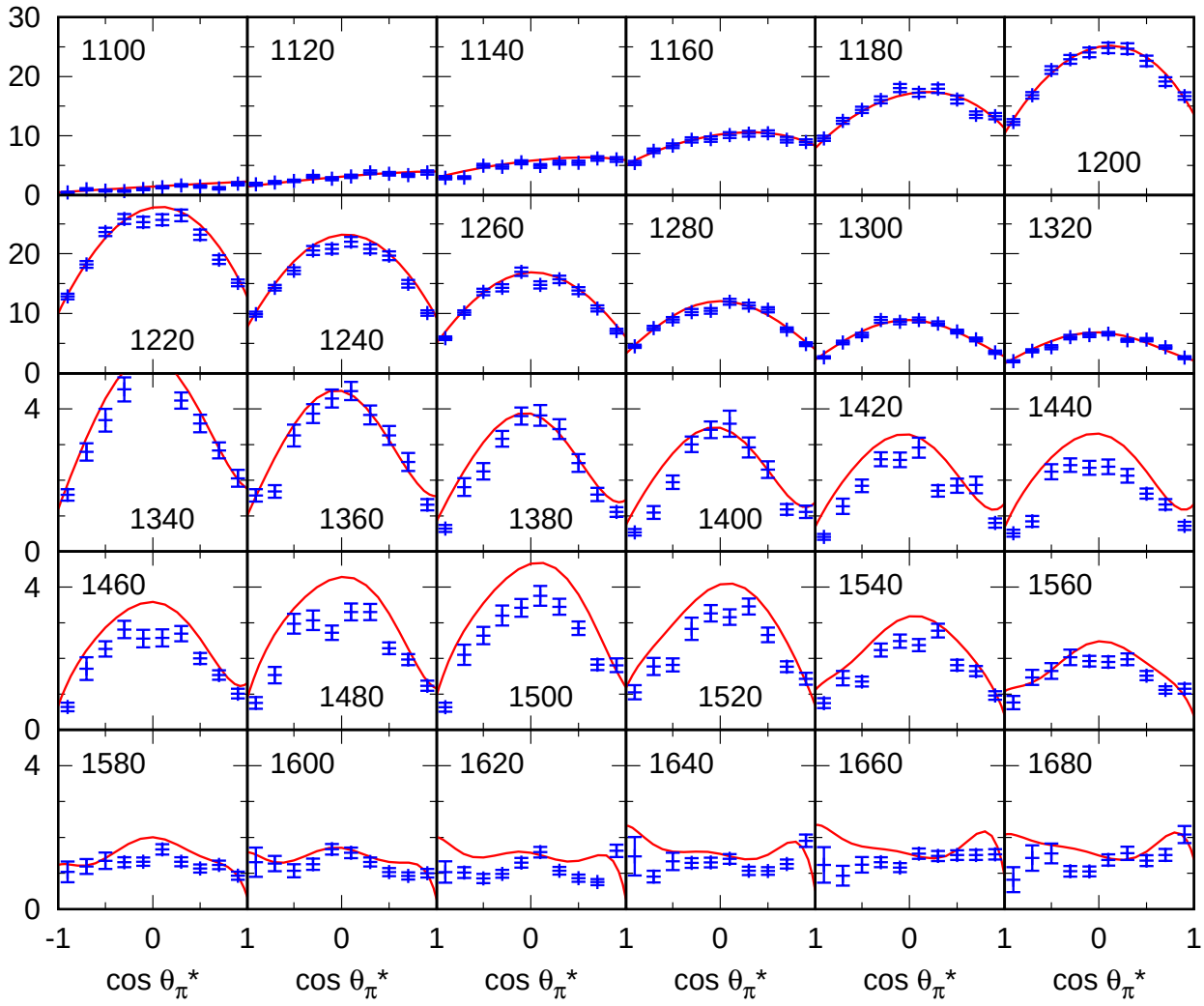

FIG. 27: Differential cross section $(\sigma_T + \epsilon\sigma_L)$ for $\gamma^* p \to \pi^0 p$ at $Q^2 = 0.4(GeV/c)^2$.

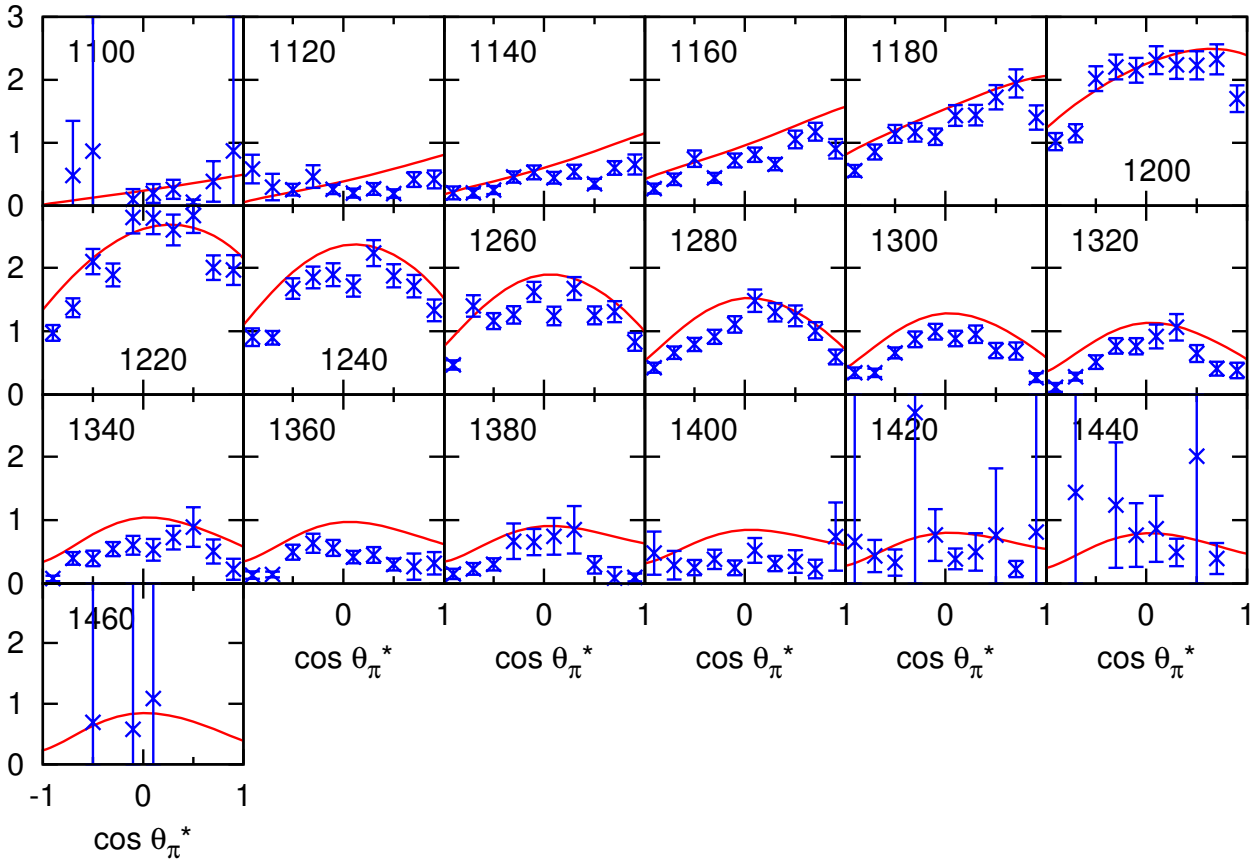

FIG. 28: Differential cross section $(\sigma_T + \epsilon\sigma_L)$ for $\gamma^* p \to \pi^0 p$ at $Q^2 = 1.76(GeV/c)^2$.

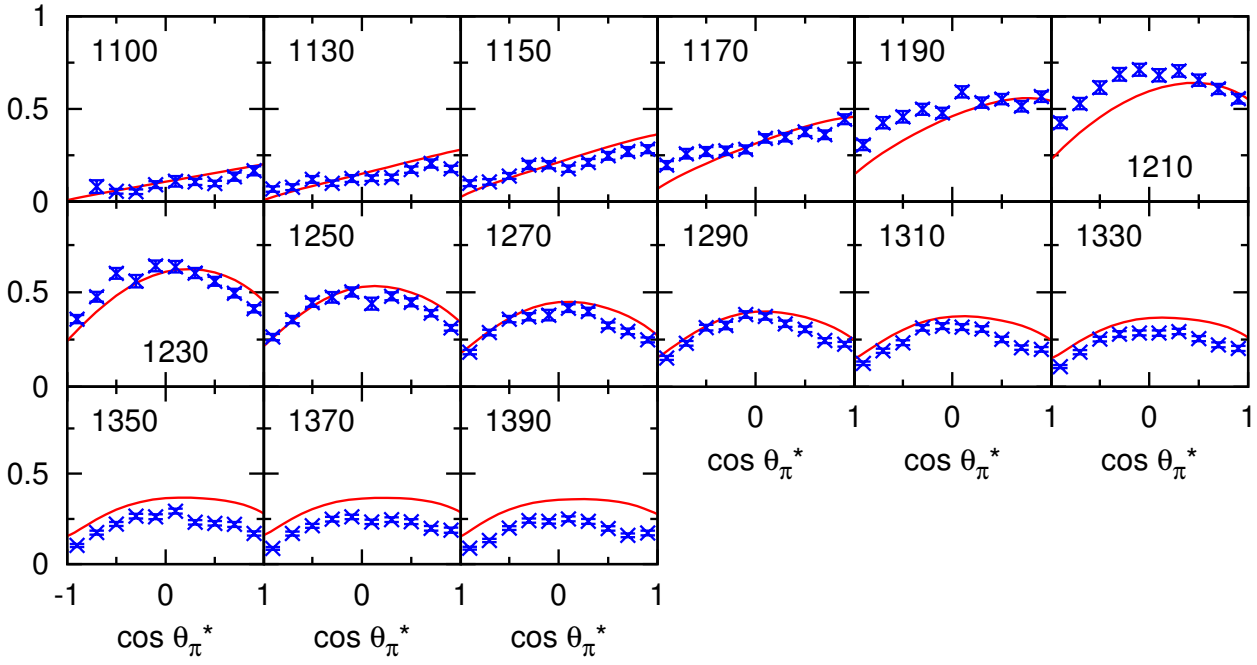

FIG. 29: Differential cross section $(\sigma_T + \epsilon\sigma_L)$ for $\gamma^* p \to \pi^0 p$ at $Q^2 = 3.00(GeV/c)^2$.

2. $\gamma^* p \to \pi^+ n$

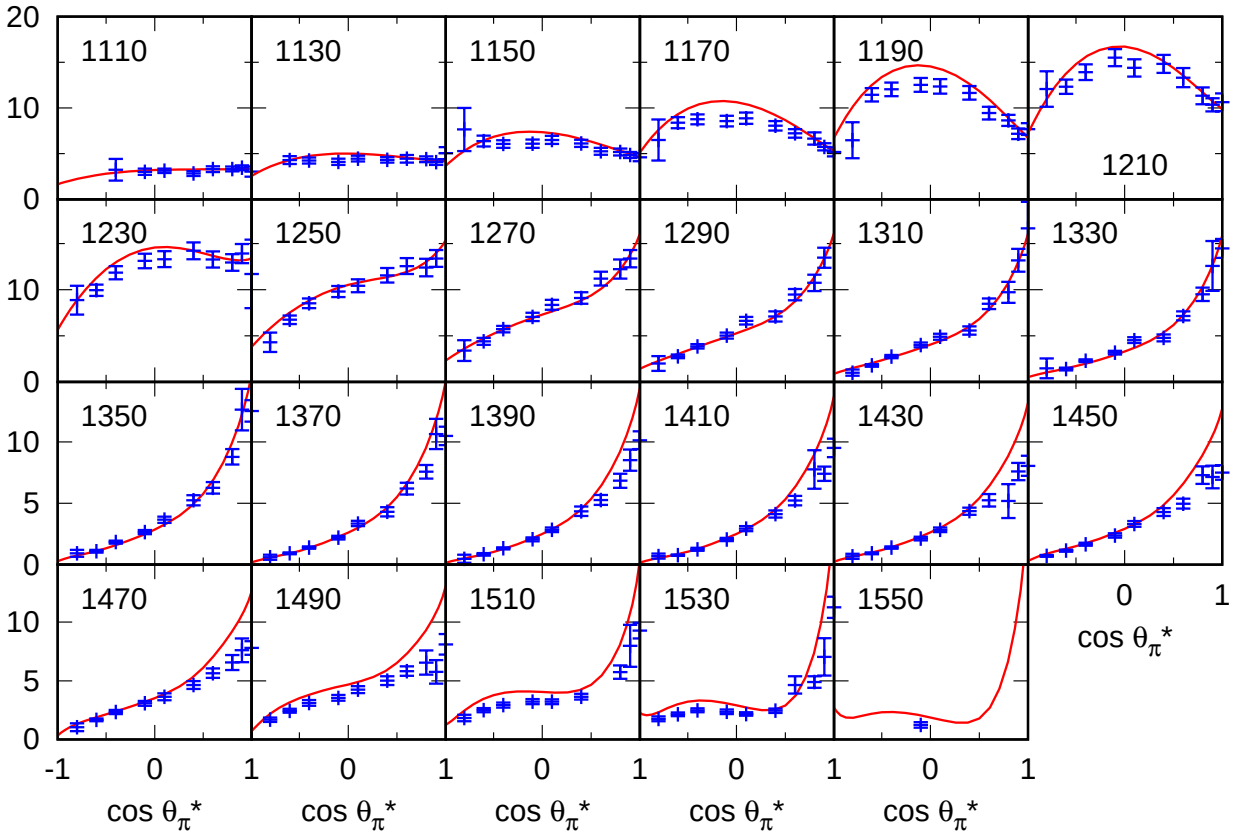

FIG. 30: Differential cross section $(\sigma_T + \epsilon\sigma_L)$ for $\gamma^* p \to \pi^+ n$ at $Q^2 = 0.4(GeV/c)^2$.

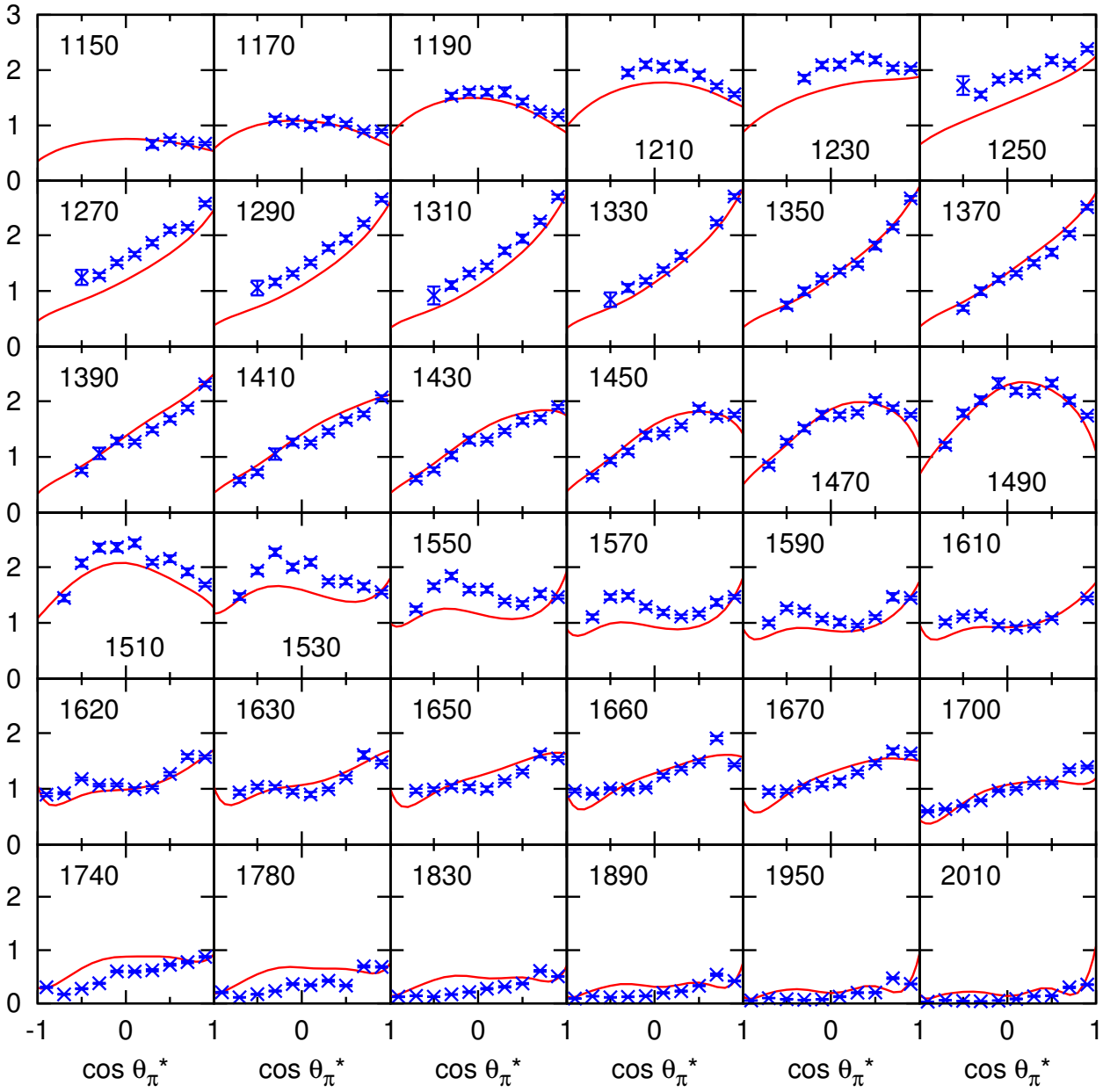

FIG. 31: Differential cross section $(\sigma_T + \epsilon\sigma_L)$ for $\gamma^* p \to \pi^+ n$ at $Q^2 = 1.76(GeV/c)^2$.

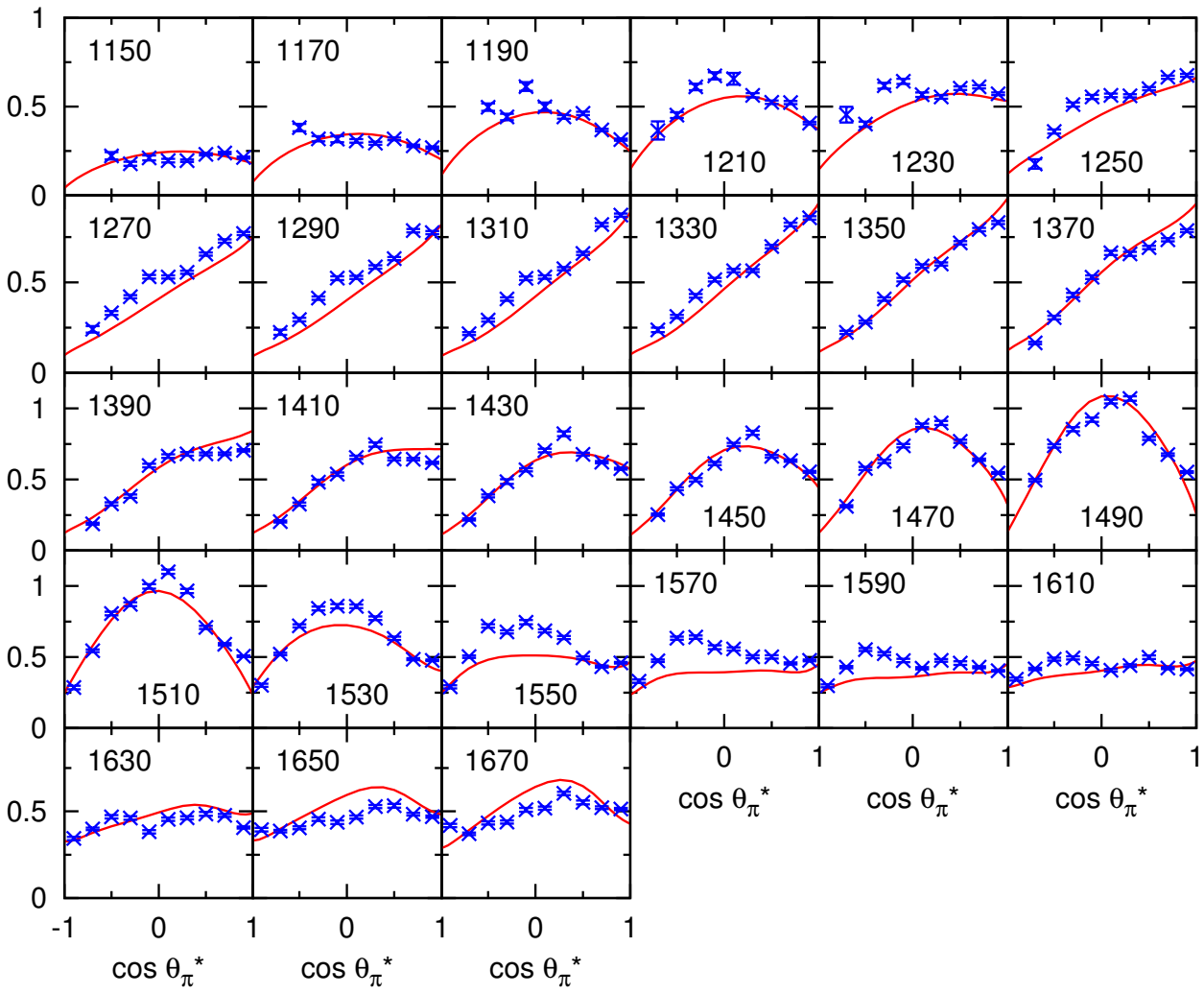

FIG. 32: Differential cross section $(\sigma_T + \epsilon\sigma_L)$ for $\gamma^* p \to \pi^+ n$ at $Q^2 = 2.91(GeV/c)^2$.

Appendix F: Inclusive cross section of $p(e, e')$

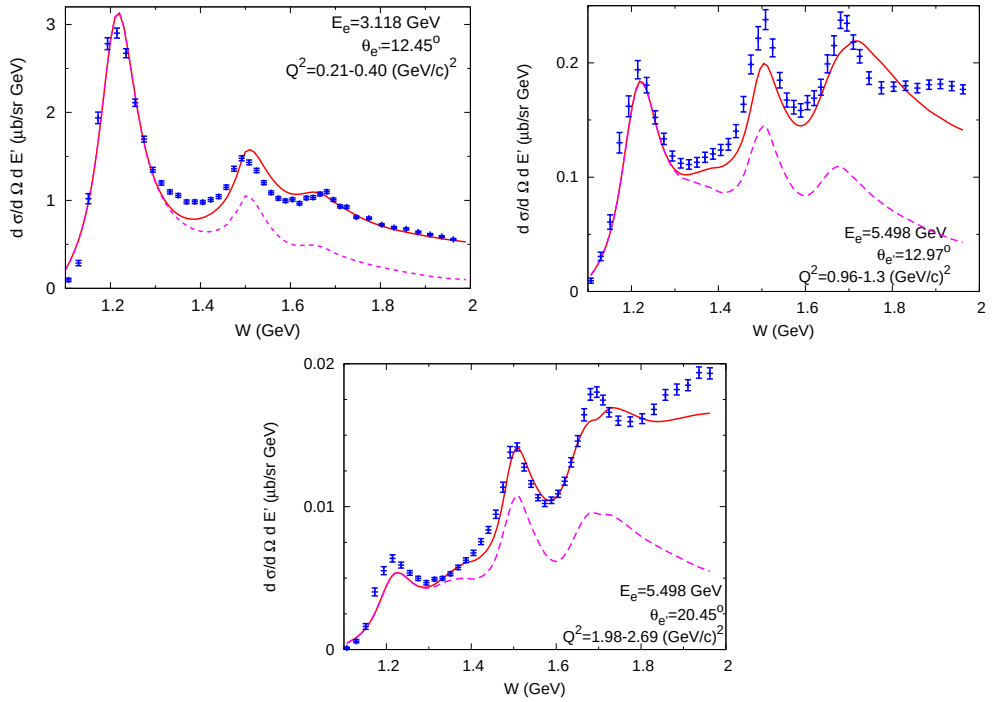

FIG. 33: Differential cross sections of $p(e, e')X$ at $Q^2 \sim 0.3, 1.1, 2.3(GeV/c)^2$. Dashed curves are from the contributions of $p(e, e'\pi)N$.

[1] Meson-exchange model of πN scattering and $\gamma N \to \pi N$ reaction
T. Sato, T.-S. H. Lee, Phys. Rev. **C34**,2660 (1996)
[2] Dynamical study of Δ excitation in $N(e, e'\pi)$ reaction
T. Sato, T.-S. H. Lee, Phys. Rev. **C63**, 055201 (2001)
[3] Extraction and Interpretation of$\gamma N \to \Delta$ form Factors within a Dynamical Model
B. Julia-Diaz, T.-S.H. Lee, T. Sato, L.C. Smith, Phys.Rev. **C75**, 015205 (2007)
[4] Dynamical coupled-channel model of meson production reaction in the nucleon resonance region
A. Matsuyama, T. Sato, T.-S. H. Lee, Phys. Rept **439**, 193 (2007)
[5] Dynamical coupled-channel model of πN scattering in the $W < 2$ GeV nucleon resonance region
B. Julia-Diaz, T.-S. H. Lee, A. Matsuyama, T. Sato, Phys. Rev. **C76**, 065201 (2007)
[6] Dynamical coupled-channel effects on pion photoproduction
B. Julia-Diaz, T.-S. H. Lee, A. Matsuyama, T. Sato, L.C. Smith, Phys. Rev. **C77**, 045201 (2008)
[7] Dynamical coupled-channel study of $\pi^- p \to \eta n$ process
J. Durand, B. Julia-Diaz, T.-S. H. Lee, B. Saghai, T. Sato, Phys. Rev. **C78**, 025204 (2008)
[8] Extraction of resonances from meson-nucleon reaction
N. Suzuki, T. Sato, T.-S. H. Lee,Phys. Rev. **C79**, 025205 (2009)
[9] Dynamical coupled-channels study of $\pi N \to \pi\pi N$ reactions
H. Kamano, B. Julia-Diaz, T.-S. H. Lee, A. Matsuyama, T. Sato, Phys. Rev. **C79**, 025206 (2009)
[10] Dynamical coupled-channels analysis of ${}^1H(e, e'\pi)N$ reactions
B. Julia-Diaz, H. Kamano, T.-S. H. Lee, A. Matsuyama, T. Sato, N. Suzuki Phys. Rev. **C80**, 025207 (2009)
[11] Double and single pion photoproduction within a dynamical coupled-channels model
H. Kamano, B. Julia-Diaz, T.-S.H. Lee, A. Matsuyama, T. Sato, Phys. Rev. **C80**, 065203 (2009)
[12] Disentangling the dynamical origin of P_{11} nucleon resonances
N. Suzuki, B. Julia-Diaz, H. Kamano, T.-S. H. Lee, A. Matsuyama, T. Sato, Phys. Rev. Lett. **104**, 042302 (2010)
[13] Extraction of P_{11} resonances from πN data
H. Kamano, S. X. Nakamura, T.-S.H. Lee, T. Sato, Phys. Rev. **C81**, 065207 (2010)
[14] Extraction of electromagnetic transition form factors for nucleon resonances within a dynamical coupled-channels model
N. Suzuki, T. Sato, T.-S.H. Lee, Phys. Rev. **C82**, 045206 (2010)
[15] Determining pseudoscalar meson photo-production amplitudes from complete experiments
M. Sandorfi, S. Hoblit, H. Kamano, T.-S. H. Lee, J. Phys. G **38**, 053001 (2011)
[16] Nucleon resonances within a dynamical coupled-channel model of πN and γN reactions
H. Kamano, S.X. Nakamura, T.-S.H. Lee, T. Sato, Phys.Rev. **C88**, 035209 (2013)
[17] Isospin decomposition of $\gamma^* N \to N^*$ transitions within a dynamical coupled-channels model
H. Kamano, S.X. Nakamura, T.S.H. Lee, T. Sato, Phys.Rev. **C94**, 015201 (2016)
[18] Dynamical coupled-channels model for neutrino-induced meson productions in resonance re-

gion
S.X. Nakamura, H. Kamano, T. Sato, Phys.Rev. **D92**, 074024 (2015)